To the Graduate Council:

I am submitting herewith a dissertation written by Viktor Chupryna entitled “Explicit Methods in the Nuclear Burning Problem for Supernova Ia Models”. I have examined the final electronic copy of this dissertation for form and content and recommend that it be accepted in partial fulfillment of the requirements for the degree of Doctor of Philosophy, with a major in Physics.

Michael Guidry, Major Professor

We have read this dissertation
and recommend its acceptance:

Dr. William Bugg

Dr. Ohannes Karakashian

Dr. Yuri Efremenko

Dr. William Raphael Hix

Accepted for the Council:

Carolyn R.Hodges
Vice Provost and
Dean of the Graduate School

Explicit Methods in the Nuclear Burning Problem for Supernova Ia Models

A Dissertation

Presented for the

Doctor of Philosophy

Degree

The University of Tennessee, Knoxville

Viktor Chupryna

December 2008

Dedication

This dissertation is dedicated to the memory of my mother

Acknowledgments

First of all I thank my major professor Michael Guidry for agreeing to take me as a student, for offering me this project and letting me work on it. His encouragement, interest in the subject of research, knowledge and experience, unique ability to formulate any problem in an extremely clear way, and readiness to help were decisive in leading me to completing this project. Fighting FLASH without the help and support of Dr. Bronson Messer, whose expertise in computing and astrophysics is impressive, would be a hopeless business for me. Each communication with him restored my hope and showed the ways to overcome new obstacles. In programming and computers I learned a lot from Jay Billings who was always ready to share his knowledge and to help me to solve many problems, even those that have nothing to do with my reseach interests. My current computer partner and officemate Elisha Feger is highly appreciated for help in computing. At the final stage of preparation of the thesis, and especially presentation and fast solution of organizational issues, I was helped by Elisha's parents to whom I express my appreciation. My thanks go also to Dr. Raph Hix who was always ready to share his knowledge. Communication with Suzanne Parete-Koon was not only interesting but also very helpful especially when we tackled together FLASH. In the very beginning of my work on this research project I made my first steps in computing and especially in learning Linux with the help of Reuben Budiardja, to whom I am thankful. All three, Reuben, Jay, and Elisha worked hard to make operative stand-alone code that was later used in FLASH. I express my thanks to Erin McMahon. My project was in fact a continuation of her research. She made my transition to it less painful. I am especially thankful to Dr. Joseph Macek whose financial support was vital for my progress. Working with him and Dr. Serguei Ovchinnikov in the field of dynamic atomic collisions was very interesting, productive, and educational. Finally I thank the Department

of Physics and Astronomy for support for all the period of my study, and especially Dr. James Parks whose help and support was not always noticeable, but always important.

Abstract

Most modern astrophysical problems such as supernova simulation require application of state-of-the-art computational tools. Despite the fact that number of nuclei included in coupled simulations tends to be small, problems such as nuclear burning networks are often part of a large set of interconnected programs that require significant computing resources. Expansion of the nuclear reaction network to realistic sizes can easily make element and energy production the leading consumer of both time and memory in simulations. Therefore, in solving nuclear reaction networks coupled to (radiation) hydrodynamics in astrophysics simulations, the development of methods capable of improving on the traditional approaches becomes important. Reactions in thermonuclear networks may exhibit huge differences in the time scales characterizing their behavior. This causes instabilities (stiffness) in the differential equations that make most standard numerical integration methods impractical. In astrophysics applications, implicit numerical integration has traditionally been used to overcome the stiffness problem. This approach is stable in typical applications, but is computationally expensive and has poor scaling behavior with network size. Thus, even the best previous calculations have been forced to use unrealistically small networks in multi-dimensional hydrodynamics simulations. Explicit flux-limited integration to cure stiffness far from equilibrium combined with asymptotic approximations used to cure stiffness in the approach to equilibrium provide an attractive alternative if they can be made fast enough and accurate enough for production use. Because of very favorable scaling behavior, the advantages of this approach are especially noticable in the case of (more realistic) large networks. The purpose of this dissertation is to evaluate the feasibility of using this new approach to couple thermonuclear networks of realistic size to 3-dimensional hydrodynamics for Type Ia supernova simulations.

Contents

1 Introduction **1**

2 Type Ia Supernovae **3**

2.1 Classification of Supernovae 3

2.2 Thermonuclear Supernovae 7

2.3 Progenitors 7

2.4 Pre-ignition evolution 8

2.5 The Explosion Mechanism and Confronting Observations 9

2.6 Standardized Candles and Cosmology 10

3 Computer Modeling of Type Ia Supernovae **12**

3.1 Hydrodynamics 13

3.1.1 Thermonuclear Flames 14

3.1.2 Thermonuclear Networks 16

3.2 The FLASH Code 18

4 Explicit Numerical Solutions of Large Thermonuclear Networks **22**

4.1 Motivation 22

4.2 Explicit Flux-Constrained Integration 24

4.2.1 The Basic Problem 24

4.2.2 The Flux-Limiting Prescription 24

4.2.3 Advantages and Limitations of Explicit Flux-Constrained Integration . . . 25

4.3 Asymptotic Flux-Constrained Integration 26

4.3.1 Non-Equilibrium Stiffness 27
4.3.2 Stiffness in the Approach to Equilibrium 27
4.3.3 Curing Stiffness in the Approach to Equilibrium 28
4.3.4 Asymptotic Approximations 28
4.3.5 Asymptotic Flux-Constrained Algorithm 30

5 Tests of Explicit Methods on Alpha Networks and under Hot CNO Conditions 32
5.1 Energy and Isotope Production in an Alpha Network 32
5.2 Hot CNO Cycle at Constant Temperature and Density 34
5.3 Large Networks under Nova Conditions 39

6 Post-Processing Tests of Explicit Methods under Type Ia Conditions 42
6.1 Post-Processing Approximations 42
6.2 Example: High-Density, High-Temperature Burns to NSE 43
6.3 Example: Gravity-Confined Detonation Conditions 46

7 Operator-Split Coupling of Realistic Networks to Hydrodynamics for the Type Ia Supernova Problem 49

8 Summary and Conclusions 54
8.1 What Has Been Accomplished in this Work 54
8.2 What Remains to Be Done 55
8.3 What New Directions Are Suggested by this Work 55

Vita 61

List of Figures

2.1 The current classification of supernovae 4

2.2 Early-time spectra for major types of supernovae 5

2.3 Late-time spectra for major types of supernovae 5

2.4 Schematic light curves for SNe of different types (subtypes) 7

2.5 The GCD mechanism 11

3.1 Comparison of scale disparities in SN Ia 15

3.2 Schematic architecture of the FLASH code (from the FLASH 2.5 User's Guide). Only the first three levels of the architecture hierarchy are shown. In the present work, we have made substantive changes to the Materials and Source terms Modules. Materials was extended with new Composition (which are components of the Equation of State module) representing the isotopic makeup of our implemented networks. Source Terms was extended by the addition of a new Burn submodule encapsulating our explicit network algorithm. 19

4.1 A simple box model 25

5.1 Energy production rate dE/dt and integrated energy production E for various levels of asymptotic approximation compared with an exact numerical integration. The asymptotic curves are labeled by the value of the tolerance parameter defining the maximum fractional violation of particle number permitted in a single integration step. These calculations used an alpha network with REACLIB reaction rates at constant temperature $T = 7 \times 10^9$ K and constant density $\rho = 1 \times 10^8$ g cm^{-3}. For tolerance parameters of 10^{-8} or smaller the asymptotic result is essentially exact over the entire integration range (compare the red dashed curve with the green solid curve). 33

5.2 Rate of energy production dE/dt as in Fig. 5.1 but for constant $T = 5 \times 10^9$ K and constant $\rho = 1 \times 10^8$ g cm^{-3}. For tolerance parameters of 10^{-8} or smaller the asymptotic result is indistinguishable from the exact result (green line) over the entire integration range, and the more generous tolerance parameters cause deviations only at the very latest times. 34

5.3 Comparison of mass fractions X for isotopes in the alpha network of Fig. 5.1. Solid lines represent exact numerical integration and dashed lines illustrate an asymptotic approximation with a particle number conservation tolerance number of 1×10^{-6}. The asymptotic and exact results are indistinguishable except for small differences at very late times. Compare with Fig. 5.4, where the asymptotic result is essentially exact over the entire time range. 35

5.4 Comparison of mass fraction X for isotopes in the alpha network of Fig. 5.1. Solid lines represent exact numerical integration and dashed lines illustrate an asymptotic approximation with a particle number conservation tolerance number of 1×10^{-8}. For this value of the tolerance parameter or smaller, the asymptotic results are indistinguishable from the exact result. The integrated energy production is also illustrated by green + symbols and is indistinguishable between the exact and asymptotic approximations. 36

5.5 Some isotopic abundances under nova (hot CNO) conditions calculated using the flux-constrained explicit algorithm. 37

5.6 Evolution of network under nova conditions. 40

5.7 Hydrodynamic profiles associated 41

6.1 Element production in a Type Ia supernova 44
6.2 Element production in a Type Ia supernova 45
6.3 Mass fractions and abundances, GCD conditions 47
6.4 Abundance evolution 48

7.1 150-isotope network coupled to FLASH 50
7.2 150-isotope network coupled to FLASH: T and dE/dt. 51
7.3 150-isotope network coupled to FLASH: E and dE/dt. 51

Chapter 1

Introduction

Supernovae are among the most violent and spectacular events that occur in the Universe. Although substantial progress has been made in understanding the mechanisms of these events, all numerical simulations of supernovae to date have of necessity employed serious limitations on the physics that could be incorporated. These limitations are partially associated with lack of fundamental input information, but ultimately are defined by shortcomings in current computational power and algorithms. As a result, it is fair to say that we have a broad understanding of supernova physics but many details of these explosions remain elusive at the theoretical level.

In addition to their intrinsic interest, supernovae are increasingly important in understanding a variety of other phenomena in astrophysics. Traditionally, they have been central to issues such as galactic chemical evolution and the understanding of elemental abundances. More recently, supernovae have assumed importance in topics of even broader cosmological interest. Perhaps the two most important examples are accumulating evidence that long-period gamma-ray bursts may be associated intimately with particular classes of core-collapse supernovae, and the role of Type Ia supernovae in the emergence of the New Cosmology, in particular their role in suggesting that the Universe is dominated by a mysterious dark energy that is causing the expansion to accelerate.

Because of their fundamental role in modern observational cosmology, understanding the mechanism of Type Ia supernovae is of particular importance (see references [1]–[13] for an overview of our current understanding of supernovae, with particular emphasis on Type Ia). As shall be described in more detail below, Type Ia supernovae are at center stage in cosmology today because they are very bright (so they can be seen at great distance) and because there is phenomenological

evidence that their intrinsic brightness can be predicted from their observable characteristics (meaning that they can be used as reliable distance indicators). It is vital that we understand the mechanism responsible for energy production in Type Ia supernovae, both because of intrinsic interest in what causes such a spectacular outburst, and because of their critical role as distance indicators in modern cosmology.

This study is devoted to a particular aspect of Type Ia supernova simulations: the coupling of the nuclear burning network that is responsible for powering the supernova to the multidimensional radiation hydrodynamics that describes the time evolution of many observables in the supernova. In particular, it was demonstrated that a new approach to the nuclear burning network permits the coupling of a more realistic network to the hydrodynamical simulation than has been possible to date. Since it is this burning network that is responsible for the energy release in the supernova, and since all Type Ia simulations to date have of necessity employed a highly truncated and schematic burning network, this work has the potential for significant impact both in understanding the mechanism for Type Ia supernovae and in shoring up the observational foundations of the emerging New Cosmology.

The organization of this thesis is as follows. A general introduction is presented in Chapter 1. Chapter 2 gives today's picture of Type Ia supernovae and their place in modern astrophysics. The status of modern computer modeling of Type Ia Supernovae and available research tools are described in Chapter 3. New explicit numerical solutions of large thermonuclear networks are described in Chapter 4. Chapter 5 is devoted to testing the explicit method presented in the previous chapter in alpha networks and in large networks under hot-CNO conditions. Post-processing testing of the explicit method under Type Ia supernova conditions is presented in Chapter 6. Finally the results of computer modeling of an operator split coupling of a realistic network to multidimensional hydrodynamics is presented in Chapter 7. The final chapter contains a summary of what has been accomplished in this work, a listing of remaining issues, and a brief discussion of possible future directions for the work presented here.

Chapter 2

Type Ia Supernovae

2.1 Classification of Supernovae

Supernovae can be divided according to observational characteristics into two broad categories: Type I and Type II (See Fig. 2.1).

With modern technology, spectra measured at early and late-times and photometric light curves are usually sufficient for reliable classification. Supernovae of Type I (SNe I) are hydrogen deficient while Type II supernovae (SNe II) spectra are dominated by strong H_α emission lines. SNe I can be divided into three classes: Ia, Ib, and Ic. In early-time spectra of SNe Ia strong Si II structure is present (most notably, $\lambda 6355$ in Fig. 2.2), while Ib and Ic subclasses do not show this line. Type Ib is characterized by prominent He I lines, especially He I $\lambda 5876$, while neither Si II nor He I can be found in SNe Ic spectra.

Light curve analysis for SNe of different types leads to the conclusion that SNe I curves are all quite similar to each other while SNe II are not simply photometrically similar to one another (See Fig. 2.4). SNe II light curves can be subdivided into two categories: one of which is similar to SNe I (it is designated as II-L on the figure) and the other has a "plateau"(II-P). The peak absolute magnitudes of SNe II-P display a broad dispersion thought to be associated with the radii (envelope sizes) of the progenitor stars, while SNe II-L tend to have uniform peak absolute magnitudes and their late-time light curves are similar. However, it is the observed uniformity of SNe Ia light curves that has important ramifications for modern observational cosmology (see Section 2.6). It is believed that SNe II, SNe Ib and Ic originate in the same basic mechanism (different from SNe Ia):

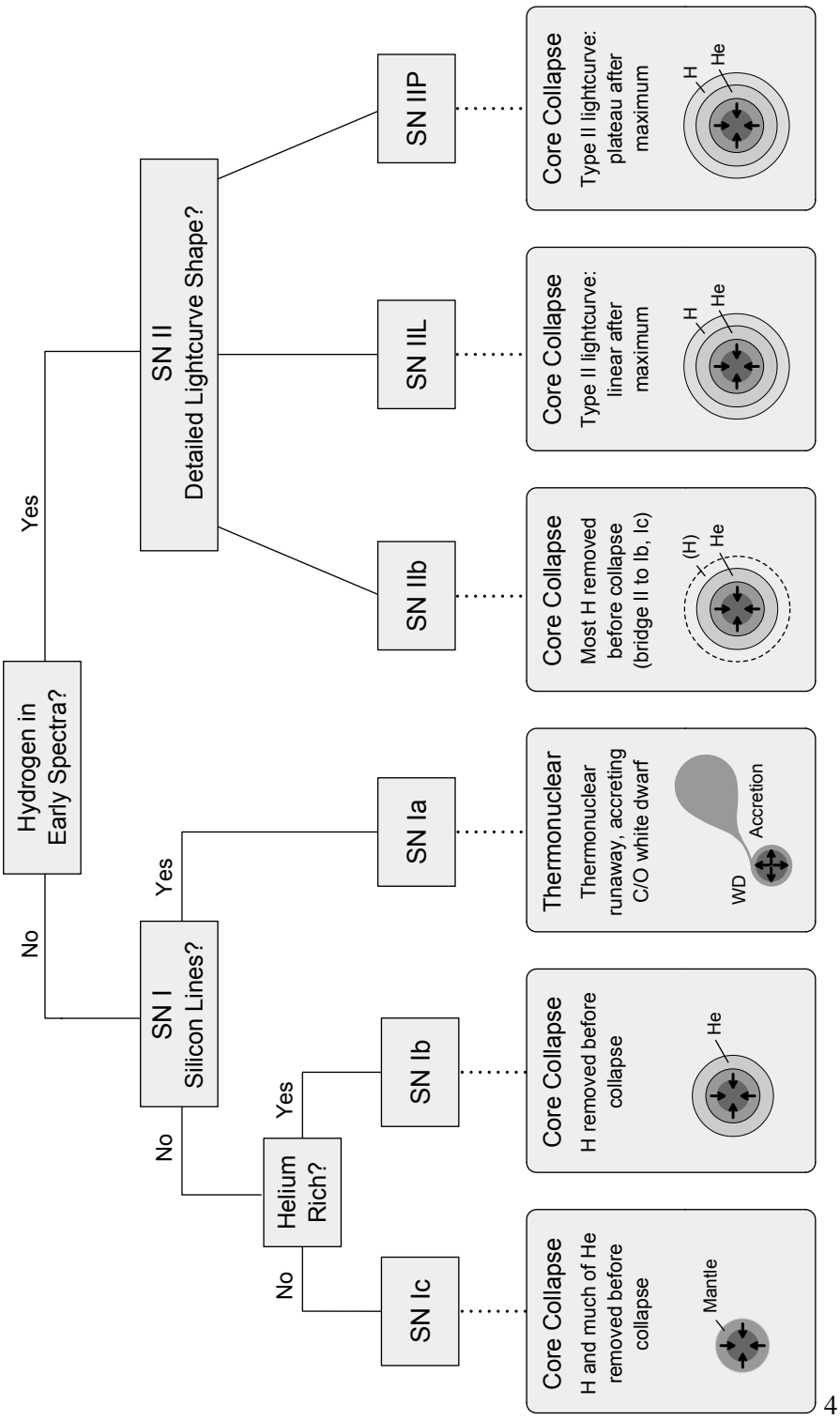

Figure 2.1: The current classification of supernovae. Type Ia SNe are connected with thermonuclear runaways on accreting WDs. Type II SNe and Types Ib and Ic are associated with core-collapse of massive stars.

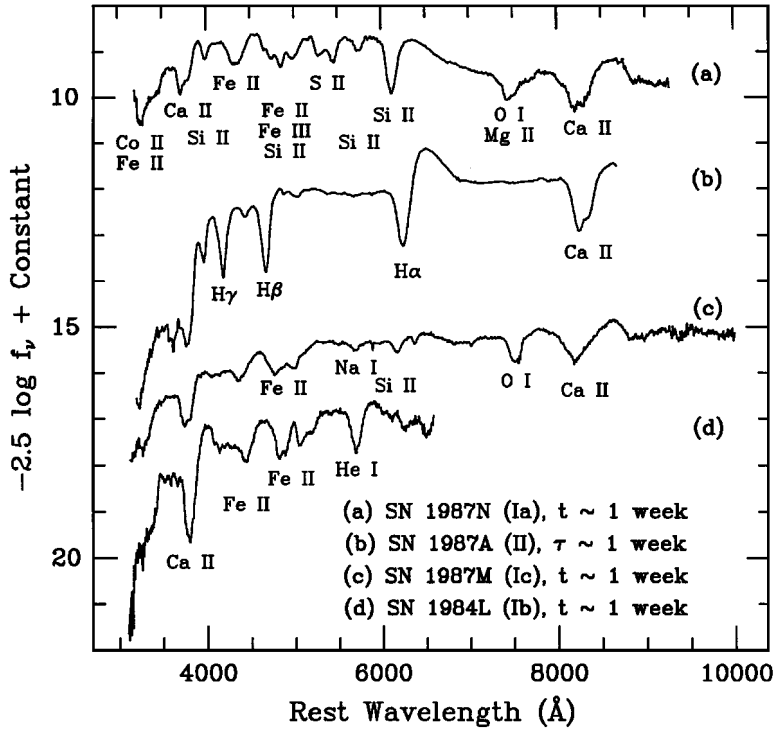

Figure 2.2: Early-time spectra for major types of supernovae [3]

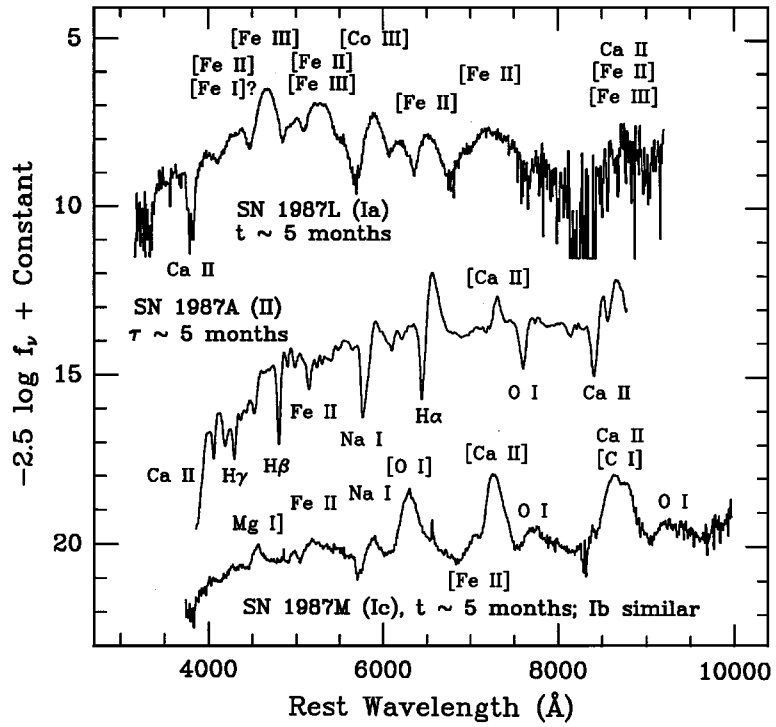

Figure 2.3: Late-time spectra for major types of supernovae [3]

they evolve from massive stars (> 8-10 $M_{\odot}$) that undergo core collapse, leaving behind a neutron star or a black hole. In the case of SNe Ib and Ic, the core physics is similar to that of SN II, except that before the explosion the progenitors were deprived of their hydrogen (Ib case) and possibly helium (Ic case) envelopes either by stellar winds or Roche lobe overflow onto a companion star.

A significant part of the optical display of SNe Ia is caused by photons from the radioactive decay of ^{56}Ni (see, for example, Ref. [14]). The amount of ^{56}Ni and the depth to which it is buried in the ejecta will affect the light curve. The composition of the ejecta and the resulting opacity are also very important, as they determine the escape parameters of radiation. The temperature dependence of the opacity is the primary factor in determining the light curve shape. The ejecta of SNe Ia form an opaque expanding sphere into which energy is deposited by radioactive decay at an exponentially declining rate. Because initially the sphere is highly opaque, the energy is mainly converted into kinetic energy and the luminosity is quite small. As time passes, the ejecta becomes more dilute and the luminosity increases. Superimposed on this changing opacity is the exponentially declining energy input. This convolution produces a definitive peak in the light curve. Shortly after the peak a considerable amount of radiation will be trapped and will begin diffusing outward. Because the energy deposition is declining very fast, the luminosity will remain at the maximum level for a while until all the stored excess energy is depleted. Finally the luminosity becomes equal to the instantaneous deposition rate. From this point forward the photon energy is primarily from the decay of the radioactive ^{56}Co in the ejecta. Thus we can talk of two stages in light curves for Type Ia supernovae: the first one occurs near peak when the luminosity first rises above the rate of energy accumulation, the second occurs when the excess stored energy is exhausted and the luminosity falls to a value equal to the instantaneous deposition. Most of the difficulty in producing light curves and spectra arises from correctly characterizing the transport and escape of the thermalized radiation. The rate of decline of light curves at later time after the maximum is close to that expected if they are powered by the decay of ^{56}Co to ^{56}Fe.

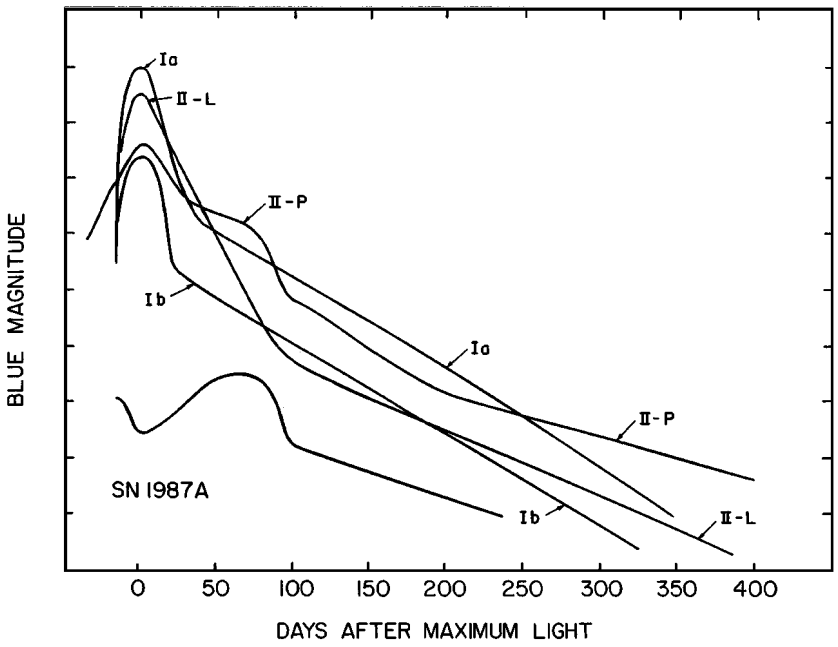

Figure 2.4: Schematic light curves for SNe of different types (subtypes) [3]

2.2 Thermonuclear Supernovae

2.3 Progenitors

For SNe Ia, the literature is dominated by three possible progenitor models: a sub-Chandrasekhar mass white dwarf (WD) undergoing a surface He flash, merging white dwarfs, and accreting carbon–oxygen WDs belonging to a binary system and reaching Chandrasekhar mass before the explosion. In the first model carbon detonation is triggered by thermonuclear runaway in an accreted He layer that drives a strong enough shock to initiate detonation in the carbon. This scenario has the advantage of having a relatively high rate of occurrence, but the exquisitely precise accretion rates required to obtain this situation instead of a nova or accretion-induced collapse makes its practical realization unlikely [1]. Also models show unobserved high-velocity Ni in the ejecta.

The second model is also called the doubly-degenerate (DD) scenario for SNe Ia. Some simulations show that it is accompanied by the gravitational disruption of the less massive star, which leads to the formation of an accretion disk around the more massive star. Later evolution is then determined by the accretion rate of the disk. Again, although the possible rate for the DD scenario

and the natural explanation for the absence of hydrogen provided by the scenario are attractive, the particulars of the mechanism and attempts to match observations have placed it in disfavor [1].

The third model is the most plausible at this point. It is generally accepted that the progenitors of SNe Ia are carbon–oxygen white dwarfs that belong to a binary system with a less-evolved companion. The WD accretes matter from the companion star and after reaching the Chandrasekhar mass limit undergoes a thermonuclear runaway initiated by an instability deep in the WD.

2.4 Pre-ignition evolution

The evolution preceding ignition constitutes an essential part of the model. The following processes, in large part, determine the energetics of evolving WDs in binaries ([1], [15]).

1. Compressional heating caused by accretion.

2. Nuclear burning. Compression and heating cause carbon burning in WDs. The burning leads to a thermonuclear runaway when $T > 5 \cdot 10^7$ K.

3. Neutrino emission. The energy loss by neutrino emission is important.

The start of the last stage of progenitor evolution is marked by the equality of energy production due to carbon burning and energy loss by neutrino emission. The locus defined by this condition in the plane of central density and temperature is known as the "ignition line." The development of a convective core that serves to deliver energy produced by carbon burning outward in the WD is very important for understanding the subsequent evolution. The convective phase lasts about 1000 years and is called the "smoldering phase," as the nuclear burning changes the internal energy of the matter little during this stage. Convection involves most of the WD mass at temperatures 6-7$\cdot 10^8$ K. At $T \sim 10^9$ K the critical temperature is reached for carbon burning. At this temperature the energy generation rate is equal to the heat conduction rate (mediated mostly by the degenerate, relativistic electrons deep in the WD core). This point defines the ignition of the thermonuclear runaway (the start of type Ia Supernova explosion). The detailed picture is of course more complicated and there are many unanswered questions concerning the physics of the evolution to this point, some of which will be discussed later.

2.5 The Explosion Mechanism and Confronting Observations

In the Type Ia explosion there is a thermonuclear burn corresponding to conversion of carbon and oxygen fuel into heavier elements by nuclear reactions that release large amounts of energy. This burn is extremely violent and involves energy and temperature scales far beyond our everyday experience, but it shares many qualitative properties with ordinary chemical burning. There is a *burning front* that proceeds through the white dwarf, with "cooler" unburned fuel in front and hot burned products (ash) behind. This burning front can be remarkably narrow—as small as millimeters. Thus there are two extremely different distance scales characterizing the explosion: the size of the white dwarf, which is of order 10^4 km, and the width of the burning front that consumes it, which can be billions of times smaller. This presents severe difficulties in accurately modeling Type Ia explosions, since standard numerical approaches to solving the equations governing the explosion cannot handle such disparate scales without drastic approximation.

In thermonuclear and ordinary chemical burning there is an important distinction associated with the speed of the burning front. If the burning front advances through the fuel at a speed less than the speed of sound in the medium (subsonic), it is termed a *deflagration wave*. In a deflagration fuel in front of the advancing burn is heated to the ignition temperature by conduction of heat across the burning front (recall that matter described by a degenerate equation of state is a very good thermal conductor, much like a metal). On the other hand, if the burn front advances at greater than the speed of sound in the medium (supersonic) it is called a *detonation wave*. In a detonation a shock wave forms and the fuel within the shock/burning front is heated to ignition temperature by shock heating.

Deflagrations and detonations can produce different isotopic abundance signatures in the ash that is left behind. The detailed observational characteristics of Type Ia supernovae (in particular, the elemental abundances detected in the expanding debris) could be accounted for most naturally if we assume that the burn begins life as a deflagration and transitions later to a detonation. This is a difficulty for the theory because although general considerations suggest that the explosion starts off as a deflagration it is not easy to obtain a transition to a detonation without some additional considerations. Thus, we believe that the proposed Type Ia mechanism is plausible in outline, but there

are bothersome details that leave some doubt about whether we understand fully the mechanism of these gigantic explosions.

One natural method to obtain a deflagration to detonation transition (DDT) has recently been posited by [16]. This "gravitationally confined detonation" (GCD) is shown schematically in Fig. 2.5. The mechanism begins with an initial single-point ignition near (but not precisely at) the center of the WD. A buoyant bubble of hot ash accelerates toward the surface of the WD, consuming stellar fuel and being shaped by fluid instabilities as it rises. The rapid ascent of the bubble toward the surface pushes the stellar material located just above the bubble. This piston reaches the stellar surface and breaks out of the WD. This material in the bubble wraps around the stellar surface (in an essentially Keplerian orbit), followed by the partially burnt bubble material. The material wraps around the star in each direction spreading in two streams along the WD surface. Both streams remain gravitationally confined to a relatively thick ≈ 1000 km layer. The flood of surface material converges at the point opposite to the bubble breakout location, forming a conical compressed region bounded by a shock. At this point in the evolution, conditions in the shocked region approach the detonation regime: the density exceeds 1.7×10^6 g cm^{-3} and the temperature is $\approx 2.2 \times 10^9$ K. The resulting detonation propagates inward through the WD surface, completely burning (i.e. to NSE) the fresh nuclear fuel it encounters. This available fuel is prodigious, as the initial deflagration only serves to burn roughly 5% of the total stellar mass. The scenario seems likely to accurately reproduce spectral observations without having to resort to an *ad hoc* invocation of a DDT. It is this particular GCD scenario that is treated below as a laboratory for our new network methods.

2.6 Standardized Candles and Cosmology

It is appropriate here to comment on the applicability of SNe Ia observations to modern observational cosmology, especially their key role as the most direct indicator that the expansion of the Universe is currently accelerating, implying that the Universe is permeated by a mysterious *dark energy* that can effectively turn gravity into antigravity.

It is well established that the properties of Type II SNe, as well as those of Types Ib and Ic, differ essentially from one sample to another. However, the properties of Type Ia SNe are quite homogeneous. Both spectra and optical light curve shapes of most of SNe Ia are similar to each

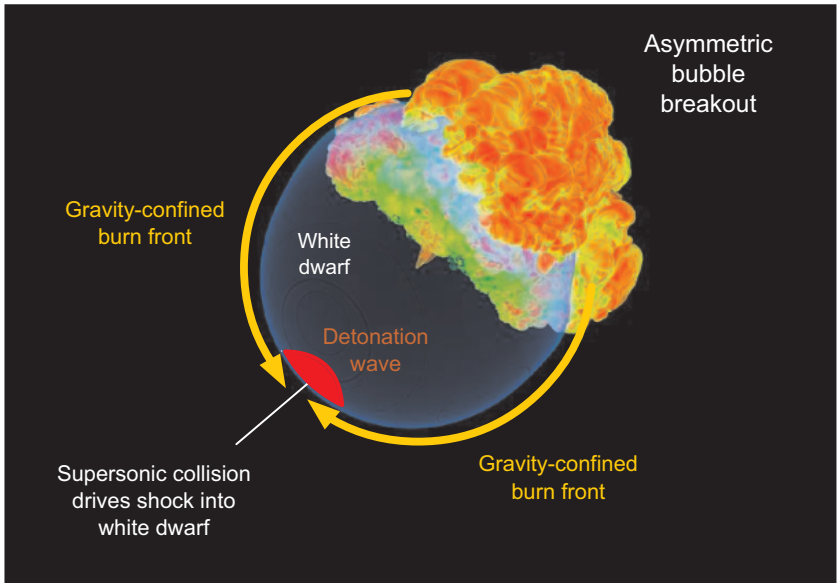

Figure 2.5: The gravity confined detonation (GCD) mechanism.

other. This resemblance of characteristics of SNe Ia attracted attention long ago and further studies led to the conclusion that SNe Ia can be used as what are termed *standardizable candles*.

A *standard candle* is an object having a very small luminosity scatter. Careful studies of SNe Ia show that, due to dissimilarities between them, they cannot be used as standard candles directly. At the same time it was noticed that there exist some correlations between spectroscopic line strength, ejecta velocities, colors, peak absolute magnitudes, and light curves. Especially useful appeared to be the very special relation between the light curve shapes of SNe Ia and their peak luminosities, which allowed normalization of the light curves to a universal one that can provide an extremely accurate determination of relative cosmological distances (see, for example, Ref. [17]).

Therefore we consider SNe Ia to be standardizable, not standard, candles. The reliable understanding of the differences mentioned above, which is vital to achieving appropriate accuracy in relating SNe Ia observations to their distance, cannot be provided by observational data only. Thorough modeling and complete understanding of physics behind the phenomena astronomers observe as SNe Ia is important to provide a firm foundation for using SNe Ia as standardizable candles. That is why computer simulation of Type Ia supernova explosions is a challenging numerical problem of extreme importance.

Chapter 3

Computer Modeling of Type Ia Supernovae

Modeling astrophysical phenomena requires coupling of physical processes that act on vastly disparate spatial and temporal scales. Furthermore, each of the physical processes described can involve processes on quite different space and time scales. For example, the time scales of thermonuclear reactions important in astrophysical processes can differ by many orders of magnitude among themselves. The spread in thermonuclear reaction rates can cause troubles with solving appropriate ordinary differential equations (ODE) that describe abundances of the elements produced and the corresponding energy released in network calculations. Beyond this, the thermonuclear time scales are often many orders of magnitude smaller than typical hydrodynamic time scales in astrophysical settings. In addition, hydrodynamic schemes must contend with distance scales ranging from millimeters (e.g. the thermal width of the flame front in Type Ia simulations) to hundreds or more kilometers (e.g. common hydrodynamical scales in WDs).

Aside from contending with these difficult, but straightforward, problems, a host of other challenges are present in astrophysical simulations. For example, shocks are ubiquitous in astrophysical settings and often require treatment with special methods. Very often there is no possibility to check

computations and associated models in terrestrial labs, since reproduction of stellar conditions (temperatures, pressures, densities, etc.) is often impossible. All these problems mean that tackling astrophysical problems requires application of state-of-the-art computational tools and software. The requirements imposed on numerical simulations for Type Ia explosions include [1]:

1. Ejecta composition and velocity should match the measured spectra and light curves.

2. The explosion mechanism should be robust: the homogeneity of SNe Ia observations requires that fine-tuning of parameters and initial conditions should not change the results fundamentally.

3. Intrinsic variability supposes that, despite being robust, the model should provide at least one parameter that could be responsible for the observed variation of explosion strengths in SNe Ia.

4. The explosion strength should be correlated with the nature of the progenitor WD (to explain the observed variations in SNe Ia as a function of host stellar population).

3.1 Hydrodynamics

FLASH is a multi-dimensional, AMR (Adaptive Mesh Refinement), reactive flow code for astrophysical problems involving nuclear burning (see Sec. 3.2 for a more complete description). It served as the "coupling laboratory" for the experiments described here. Our primary modification is the replacement of the standard thermonuclear burning module(s) with a new one implementing the explicit flux-constrained asymptotic burning algorithm. The equations solved by FLASH (see, for example, Ref. [18]) connect fluid mass density ρ, its velocity $\vec{v}$, pressure P, total internal energy E and kinetic energy per unit mass ε. In the FLASH code this corresponds to Euler's equations for compressible gas dynamics:

$$\partial\rho/\partial t + \nabla\cdot\rho\vec{v} = 0, \tag{3.1}$$

$$\partial\rho\vec{v}/\partial t + \nabla\cdot(\rho\vec{v}\vec{v}) + \nabla P = \rho\vec{g}, \tag{3.2}$$

$$\partial\rho E/\partial t + \nabla\cdot(\rho E + P)\vec{v} = \rho\vec{v}\cdot\vec{g}, \tag{3.3}$$

$$E = \varepsilon + \frac{1}{2}v^2, \tag{3.4}$$

where $\vec{g}$ is the acceleration due to gravity and t is the time coordinate. An equation of state (EOS) closes the hydrodynamics equations. One simple possibility is

$$P = (\gamma - 1)\rho\varepsilon, \tag{3.5}$$

which connects pressure P and density ρ. (Note that the EOS used in these studies is more complicated, being appropriate to describe degenerate conditions present in WD matter). It is also common to add the continuity equation for flows of each nuclear species

$$\partial \rho X_l / \partial t + \nabla \cdot \rho X_l \vec{v} = 0, \tag{3.6}$$

under the condition that the mass fraction X_l of the lth species satisfies

$$\sum_l X_l = 1. \tag{3.7}$$

A standard notation is used here:

$$X_l = \frac{N_l A_l}{\rho N_A}, \tag{3.8}$$

$$Y_l = \frac{X_l}{A_l} = \frac{N_l}{\rho N_A}, \tag{3.9}$$

where N_l is a number density of species l, N_A is Avogadro's number, and Y_l is a mole fraction or abundance of species l.

3.1.1 Thermonuclear Flames

Detonation and Deflagration

Because numerical simulations of turbulent burning often involve length scales differing by many orders of magnitude they have always presented a challenge for simulations. In the case of Type Ia supernovae, the sizes of representative bubbles can range from 10^7 cm (the largest ones) down to

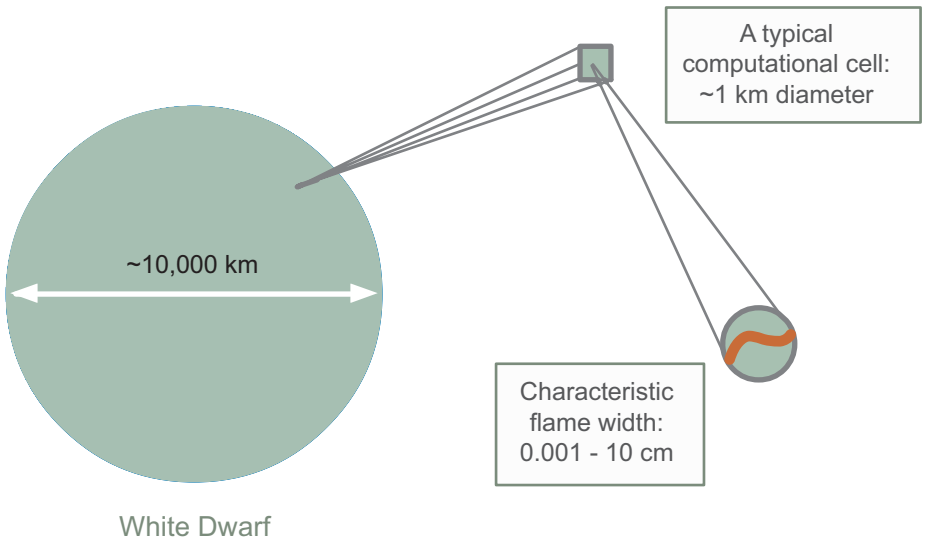

Figure 3.1: Comparison of scale disparities in Type Ia supernova simulations.

10^{-4} cm (the macroscopic Kolmogorov scale) [19]. In another example, the thickness of the flame can differ from the radius of a WD by 10-12 orders of magnitude [20]. Figure 3.1 compares the large scale disparities that characterize a Type Ia supernova simulation.

There are no computers capable of resolving this range of scales. That is why one has to resort to statistical or scaling approximations in order to formulate a subgrid model capable of representing burning on unresolved scales. Models attempt to reproduce two different regimes of thermonuclear burning in WD: subsonic deflagration and supersonic detonation. The regimes differ by the mechanism of propagation of the reactive wave. A deflagration involves heat conduction or turbulent mixing while a detonation involves shock compression. In both cases the energy is generated by the same thermonuclear reactions. Currently in the most favorable models the explosion starts as a deflagration close to the center of the star. Unstable blobs of hot burned material subject to the Rayleigh-Taylor instability move upward, as the hot ash is buoyant in the cold fuel of the WD. At the flame interface shear-induced turbulence occurs, further wrinkling the flame front. This increases the surface area of flamelets and thus the rate of fuel consumption and the total energy generation rate of the turbulent front. The turbulent flame speed becomes larger than the laminar speed. In fact, the turbulent flame speed, being roughly equal to the Rayleigh-Taylor speed, becomes independent of the laminar speed and therefore of the microphysics of burning and diffusion, and scales only with the velocity of the largest turbulent eddy. Currently, the distributed burning regime in WDs is

often wholly neglected in full-scale SNe simulations, as nuclear burning, diffusion, and turbulent mixing in the flame front cannot be properly described by simplified procedures. Problematically, it is precisely in this regime where a transition from deflagration to detonation may happen. Accurate determination of this transition is necessary to provide simulation data in good agreement with observations.

3.1.2 Thermonuclear Networks

Coupled Differential Equations

Thermonuclear burning in stars is not only a source of energy, but also a mechanism for element production, providing an explanation for the origin and evolution of chemical elements in the universe. Abundances of elements and thermonuclear energies are obtained as a result of the integration of ODEs describing coupled thermonuclear reactions. A correct treatment of thermonuclear energy generation is a costly simulation process in both memory and time. Isotopic abundances are stored at each grid point and memory requirements can be quite restrictive for 3D hydrodynamical problems, even if modern computational tools are used. Nuclear reaction networks are composed of a system of stiff ODEs. Stiff differential equations are equations with large variation in their rate constants. They present serious stability issues and generally must be solved by special methods, often involving implicit, iterative techniques. If the number of isotopes becomes greater than about 30, computation of evolving isotopic abundances by solving the ODEs in fully-coupled reactive flow codes can dominate the total cost of the model. A common trade-off is to evolve a limited number of abundances and at the same time to find an approximate value for the thermonuclear energy generation. In many cases, particularly for SNe Ia, high precision in the total energy is very important since it is vital in evaluating the validity of the model used (and eventually to provide a theoretical justification for considering SNe Ia as standardizable candles). Also, some measure of the precision of the isotopic profile is required to match observations. In this context, the search for methods that can compete with traditional approaches for solving stiff ODEs is important.

In a Lagrangian formulation and restricting ourselves to two-body reactions for simplicity of discussion, nuclear burning can be described by

$$dY_i/dt + \nabla \cdot (Y_i \vec{V}_i) = \dot{R}_i, \tag{3.10}$$

where

$$\dot{R}_i = \sum_{j,k} Y_l Y_k \lambda_{kj}(l) - Y_i Y_j \lambda_{jk}(i), \tag{3.11}$$

and where

- Y_i is a specific abundance of isotope i,
- $\dot{R}_i$ is the total reaction rate caused by binary reaction,
- λ_{kj} and λ_{jk} are creation and destruction reaction rates, respectively,
- $\vec{V}_i$ are mass diffusion velocities (pressure, temperature, abundance gradients, etc. taken into account in dealing with mass diffusion processes).

In the work presented here we will employ an operator-splitting approximation. In such an approach, one updates the network for a short interval at fixed hydrodynamic conditions, then uses the network results to update the hydrodynamics, then updates the network using the updated hydrodynamics results, and so on. The set of thermonuclear network differential equations in this case can be written as

$$dY_i/dt = \dot{R}_i. \tag{3.12}$$

This set of equations constitutes a reaction network. The reaction network and the hydrodynamics are coupled because the rates in the reaction network are strongly dependent on the hydrodynamical variables and the reaction network, in turn, modifies the energy and composition variables entering the hydrodynamics. This coupling is particularly strong in a Type Ia supernova because essentially the entire energy of the explosion (of order 10^{51} ergs) originates in the thermonuclear reaction network.

Stiffness and Traditional Implicit Solutions

As was mentioned earlier, the element production process (thermonuclear burning process) is described by stiff ODEs. It is rather difficult to give a rigorous definition of stiffness. That is why in the literature in different places it is defined differently, though the nature of stiffness is perfectly understandable qualitatively and is associated primarily with numerical stability rather than with the accuracy of computations. One definition states that "stiff equations are the equations where certain implicit methods ... perform better, usually tremendously better, than explicit ones" [21]. As noted earlier, stiffness typically occurs in equations that have rate coefficients differing by many orders of magnitude. Nuclear reaction networks in particular are often inherently extremely stiff. (General methods for solving stiff differential equations in stellar hydrodynamics are surveyed in [22].) Today in element production problems implicit methods for solving stiff ODEs are the most widely used. It is not clear whether substantial (orders of magnitudes) increases in speed and efficiency can be realized by improvement of standard implicit solvers.

For realistic coupling of nuclear burning networks to hydrodynamics for astrophysical simulations, it will be necessary to couple networks containing hundreds or even thousands of isotopes to the hydrodynamical simulation. Under those circumstances, element production networks would dominate in the simulation time and it is advantageous to explore possible approximation schemes for coupling nuclear burning to hydrodynamics that allow networks of realistic size to be implemented. In the next section I describe a new explicit flux-constrained asymptotic approach to nuclear burning networks that obtains an approximate solution to the coupled ODE problem quickly and predicts the energy production accurately while scaling very gently with network size.

3.2 The FLASH Code

The FLASH code is a parallel, adaptive-mesh simulation code for studying multi-dimensional compressible reactive flows in astrophysical environments [18]. FLASH is implemented mostly in Fortran 90 and uses the Message-Passing Interface library to achieve portability. FLASH makes use of modern object-oriented software technology that allows for minimal effort to swap or add physics modules (see Fig. 3.2).

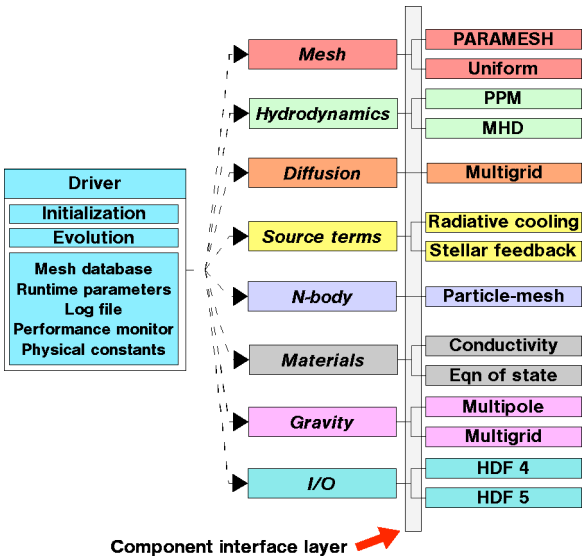

Figure 3.2: Schematic architecture of the FLASH code (from the FLASH 2.5 User's Guide). Only the first three levels of the architecture hierarchy are shown. In the present work, we have made substantive changes to the Materials and Source terms Modules. Materials was extended with new Composition (which are components of the Equation of State module) representing the isotopic makeup of our implemented networks. Source Terms was extended by the addition of a new Burn submodule encapsulating our explicit network algorithm.

The source code includes several available modules. Combining different modules leads to different applications. Each module consists of three major components: a configuration layer, an interface layer, and an underlying algorithm. When an application is set up the necessary information concerning module dependencies, default sub-modules, library requirements, runtime parameters definitions, etc. are stored in text files called Config which are parsed by setup, which is a source configuration script. After running setup the user builds an exectable with a single invocation of make. In addition to Config files, makefiles for modules are written. The major difference between the interface layer and the algorithm is in the way they access data. Interface layer routines (wrapper functions) can communicate with FLASH database module directly to access grid data. The FLASH architecture is designed in such a way so that new modules can be added straightforwardly to the code with minimal impact on other modules. Flash modules publish an effective set of public methods to clients. The public methods are expressed by sub-modules. Typically each module represents a different class of solver (e.g., hyperbolic solvers for hydrodynamics, ODE solvers for source terms). Algorithms must communicate data using a function argument list.

We have exploited this architectural design in our investigations, where we were able to confine our modifications to only two FLASH modules: Composition (a submodule of Equation of State) and Burn (a submodule of Source Terms). Nevertheless, we make use of much of the rest of the code infrastructure, especially the hydrodynamics module.

The hydrodynamics module is designed to solve Euler's equations for compressible gas dynamics to which an equation of state (EOS) as well as equations for reactive flow for each nuclear species are added. The equations are solved using a version of the Piecewise Parabolic Method (PPM) [23]. The variables like gas density, fluid velocity, internal energy, and mass fractions of each nuclear species are specified. Pressure and temperature can be found using an EOS. We use the Helmholtz EOS packaged with FLASH [24]. It includes many contributions from the relevant physics. The total pressure and internal energy can be written as:

$$p_{tot} = p_{rad} + p_{ion} + p_{ele} + p_{pos} + p_{coul}, \tag{3.13}$$

and

$$e^{int}_{tot} = e_{rad} + e_{ion} + e_{ele} + e_{pos} + e_{coul}, \tag{3.14}$$

where the subscripts at the right-hand side indicate the contributions from radiation, ions, electrons, positrons and Coulomb corrections, respectively. The radiation part is treated as a blackbody in local thermodynamical equilibrium, the ion part as an ideal gas, and electrons and positrons in the non-interacting Fermi gas formalism. The detailed formulae for each term can be found in [18]

The nuclear burners available in the stock FLASH Source Terms module include a handful of implicit networks: a seven-isotope network, a couple of 13 isotope networks with the inclusion of some heavy elements, a 19 isotope network, and a 17 isotope hydrogen burning network. All of these networks are "hardwired" (the species and rates are specified explicitly in the source code and set at compile time). The major consideration behind the use of hardwired networks is to minimize the computational time. We have added a new Burn module to FLASH encapsulating our new explicit method (described elsewhere in this dissertation).

This addition required an additional modification: a corresponding new Composition module had to be added incorporating the full set of nuclei evolved by our new Burn module. The new Composition module basically contains a list of the nuclei involved in the network included in the

new Burn module, along with nuclear masses and other nuclear data. The interface layer for the module produces "slots" in the main FLASH database structure (which is statically allocated at compile time). This allows the Hydrodynamics module access to this information for advection of species, for example, as well as providing the Burn module the basic information it is intended to evolve.

Chapter 4

Explicit Numerical Solutions of Large Thermonuclear Networks

In this chapter we take up the issue of developing stable explicit methods as alternatives to the solution of large thermonuclear networks by standard implicit means.

4.1 Motivation

Basic ideas describing the explicit approach for integrating large stiff reaction networks that we shall employ here are described in Ref. [25–27]. Discussions in these works are carried out in very general terms of fluxes between sources and sinks which are referred to as *boxes*. The whole system of sources, sinks, and boxes is called a *reaction network*. Our interest and emphasis will be of course on thermonuclear reaction networks among nuclear isotopes in astrophysics, which can be considered a specific case of the general approach. Such systems are usually represented by a set of coupled ordinary differential equations (ODE) describing a continuous flow of population through the boxes. As we mentioned earlier, since reaction rates in astrophysics may differ by many orders of magnitude, such sets are termed *stiff systems*. Loosely, stiff systems are characterized by having at least two timescales in the system that differ by many orders of magnitude [28–31].

For stiff sets of ODE usually timesteps are constrained not by accuracy requirements but by numerical stability restrictions. Explicit numerical integration of stiff systems is often impractical

since stability requirements make timesteps too small for obtaining efficient solutions (see, for example, Refs. [30, 31]). To solve this problem, the most common approach is to switch to implicit integration, which gives stable solutions and permits stable relatively large timesteps, but has large computational overhead within each step.

In principle every box in a reaction network might be connected to every other box in the system by a reaction flux but practically the connection is strong only for a very limited number of boxes in most physical applications. These restrictions on the coupling of boxes imply that the matrices appearing in iterative implicit solutions are sparse. In implicit algorithms the time is mostly consumed by numerical matrix transformations. In a typical case more than 90% of the processor time is spent in matrix manipulations [22,32]. The efficiency of implicit methods will strongly depend on the size of the networks. Increasing the size of the network increases the time required for implicit solutions, and in typical cases of working codes in astrophysics this dependence is from quadratic to cubic. Therefore implicit algorithms for solving stiff systems do not scale very gracefully to larger networks.

In many application requiring large networks the reaction network is only a part of a larger problem. In astrophysics, conditions in the network are controlled by multi-dimensional hydrodynamics that determines (for example) temperature and density. On the other hand, the network influences the hydrodynamic evolution through energy production and changes in composition. Taking into account the discussion above concerning restrictions on the computations and the complexity of practical problems, the usual approaches are very time-consuming and not many calculations have attempted to couple the element and energy production strongly to hydrodynamics using networks of realistic sizes. Usually small networks are coupled to the hydrodynamical simulations to provide important information like energy production that may be correct in some averaged sense. At the next stage a more complete network is run in a separate "post-processing" step where fixed hydrodynamical data computed using the small network are used to compute the changes in populations with time.

4.2 Explicit Flux-Constrained Integration

Two major problems in treatment of reaction networks of realistic sizes can be identified: (1) stability requirements force the use of implicit solutions, and (2) practical working codes often do not exploit the sparseness of coupled systems very efficiently. A new method of solving large networks that is based on explicit but stable manipulations of populations will be introduced in this chapter that we term *asymptotic flux-constrained integration*. It will be shown later that the new method reproduces the results of the traditional approaches. The properties of the new method may make it particularly suitable to large-scale computing applications. Investigation of whether this is so in practical problems will be the central theme of this dissertation.

4.2.1 The Basic Problem

Let us consider a coupled set of N ordinary differential equations

$$\frac{dY_i}{dt} = \sum_j F_{ij}, \tag{4.1}$$

where $Y_i (i = 1 \ldots N)$ describe the dependent variables (typically measures of abundance), t is the independent variable (often the time), the fluxes between species i and j are given by F_{ij}, and the sum for each variable i is over all variables j coupled to i by a non-zero F_{ij}. Representing sources and sinks of flux by boxes, with the arrows representing non-zero flux links between them, we can connect the differential equations given in Eq. 4.1 with Fig. 4.1. This simple 4-box representation can be generalized to sets of coupled equations describing thousands of boxes and tens of thousands of fluxes. The fluxes F_{ij} entering (4.1) may in the simplest cases be expressed as the product of a rate constant and the population of a single box, but can also be used to describe more general cases of non-linear behavior of fluxes as functions of time, for example.

4.2.2 The Flux-Limiting Prescription

The basic ideas of the explicit flux-constrained algorithm grew conceptually from the observation that physically thermonuclear networks evolve discrete (countable) populations. This has the immediate physical implication that (because the flux out of a box is proportional to a physical population

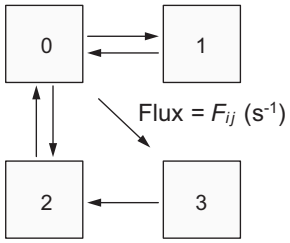

Figure 4.1: A simple box model.

of the box), it can never be negative. In the large particle-number limit approximation of such an algorithm we should recover the usual set of coupled differential equations, but we may seek to preserve this physical property by requiring that no flux F_{ij} out of box i can be smaller than zero. Detailed study demonstrates that such an algorithm is equivalent to forward Euler finite differencing, but supplemented by the elementary flux constraint

$$F_{ij} \rightarrow \max(F_{ij}, 0) \equiv \tilde{F}_{ij}. \tag{4.2}$$

That is, explicit forward Euler integration, which is highly unstable in the presence of stiffness, achieves extreme stability in the presence of stiffness through the simple prescription of replacing in each timestep any negative value of F_{ij} with zero. We shall refer to explicit Euler integration subject to this constraint as *flux-constrained explicit Euler integration*. It is important to note that this algorithm permits negative populations, but does not permit them to propagate by virtue of the flux constraint; thus, it conserves particle number.

4.2.3 Advantages and Limitations of Explicit Flux-Constrained Integration

Systematic study of this explicit flux-limiting algorithm applied to the solution of large, sparse reaction networks has demonstrated that it has some highly desirable properties:

1. The algorithm decouples stability and accuracy issues for the stiff system. The algorithm is stable because it reproduces the natural way of evolving discrete populations preventing negative populations from propagating in the network.

2. The algorithm employs the sparseness of the system perfectly since the fluxes follow only the paths of non-zero transition probability; there is a possibility to exclude from consideration flux links that are smaller than a problem-specific threshold in a numerically stable way.

3. The scaling of the algorithm with size of the network for sparse systems is linear; the time required for computing large networks often is not much larger than that required for a small network. Implicit solvers on the contrary commonly scale with the size of the network from quadratically to cubically.

4. A trade-off of accuracy against computing time is allowed by the explicit flux-constrained algorithm; it is independent of stability issues. This means that the computations can be adjusted in a stable way to optimize the required accuracy for the problem versus computing time. Even for very aggressive timesteps the physical characteristics established mostly by stronger populations tend to be reproduced well.

This method will be shown in the next Chapter to give an accurate, stable, and efficient solution of large networks that are of considerable practical importance in astrophysics such as those associated with hot-CNO burning in nova explosions. However, it does not deal well with approach to equilibrium. Since many of the problems in astrophysics that require large networks (for example, Type Ia supernovae) involve significant periods of near-equilibrium conditions, this limits the applicability of the explicit flux-constrained algorithm. In the next section we will outline a further development that will extend this explicit approach in a way much more suited to systems approaching equilibrium.

4.3 Asymptotic Flux-Constrained Integration

Because of overall simplicity and economy, and highly favorable scaling with network size, we have seen that it is desirable to integrate large, complex networks with explicit methods. To do so requires overcoming formidable numerical stability problems for explicit methods that are referred to generically as *stiffness*. As suggested above, the nature of stiffness is different for networks that are far from equilibrium compared with networks approaching equilibrium. This implies that the modifications of standard explicit methods required to stabilize them when stiffness is encountered

far from equilibrium (for example, the flux-limiting approach described in the previous section) must be altered when the same network approaches equilibrium.

4.3.1 Non-Equilibrium Stiffness

In the explicit flux-constrained integration method one systematically prohibits the propagation of "negative flux" (flux *out* of a box that is negative, which originates in box populations that have become negative). This goes a long way toward stabilizing explicit integration (allowing timesteps much larger than would be allowed in a normal explicit method for large sparse networks), because a major source of stiffness instability is the coupling to the rest of the network of populations that become slightly negative because of numerical errors. (This change in sign turns normally exponentially decaying terms highly unstable exponentially-growing terms.) For example, this method allows an efficient explicit integration of networks containing of order 1000 isotopes under nova conditions, with stable explicit timesteps that are 10^5 or more times as large as would be stable with normal explicit methods, as we shall demonstrate in the next chapter.

4.3.2 Stiffness in the Approach to Equilibrium

The minimal explicit flux-constrained method encounters efficiency problems in the approach to equilibrium for complex networks because the maximum stable timestep shortens and eventually tends to the limit set by normal explicit integration as equilibrium is approached. The reason for this behavior is also stiffness, but in a somewhat different guise than the mechanism described above. In the approach to equilibrium the population of a box is a delicate balance between a total flux F^+ populating the box and a total flux F^- depleting it. Very near equilibrium the difference $F = F^+ - F^-$ becomes orders of magnitude smaller than F^+ or F^- and small numerical errors in F^+ or F^- can produce large errors in the difference F. Because of the population coupling in complex networks, this error propagates and compromises the accuracy of the network unless the timestep is sufficiently short that the difference F is computed accurately for each population in the network. But this restriction means that the maximum timestep is set by the largest fluxes (that is, the largest stable timestep is determined by the inverses of the highest rates); this lands us back in

the explicit integration conundrum that the maximum stable timestep is set by the fastest transitions, even if the primary interest is in quantities that are varying on a much longer timescale.

Thus, in the approach to equilibrium the problem with explicit integration is not propagation of negative fluxes directly, but an unacceptable loss of accuracy that may occur even before any populations become negative. However, this is still a stiffness issue because it involves stability in systems with widely-varying timescales: we may view the approach to equilibrium as defining a longest timescale in the system that tends to *infinity,* implying that any (finite) rate for individual transitions in the system is very short compared to the timescale of primary physical interest (that for approach to equilibrium). Thus, any system close enough to equilibrium can be expected to exhibit this stiffness instability, even if there are not large differences in the rates for individual transitions in the network.

4.3.3 Curing Stiffness in the Approach to Equilibrium

Because stiffness instability in the approach to equilibrium need not be caused directly by propagation of negative flux, it cannot be cured fundamentally by the flux-constrained explicit prescription (the flux-limiting constraint may *help* in prolonging stability closer to equilibrium than would be the case for normal explicit methods, but it cannot cure the basic problem). However, as we now demonstrate, we may deal more efficiently with the approach to equilibrium if we extend the explicit flux-constrained integration method in a manner that turns the approach to equilibrium from a liability into an asset. We may do so by identifying particular conditions under which some of the differential equations in the network have an approximate solution that may be specified analytically, and using that information to remove the stiffest equations from the general numerical solution, thereby improving the overall stability of the network. In the following section one specific possibility for accomplishing this is discussed. (The general basis for the approximations examined below is discussed in Ref. 31).

4.3.4 Asymptotic Approximations

The general form of the differential equations that we must solve is

$$\frac{dy_i}{dt} = F_i^+ - F_i^- \tag{4.3}$$

where F_i^+ is the total flux increasing the population y_i and F_i^- is the total flux depleting the population y in a given timestep. For an N-species network there will be N such equations in the populations y_i, generally coupled to each other because of the dependence of the fluxes on the right side on the different y_i, but for simplicity we will not display the i index explicitly in many of the following equations.

Generally, F^+ and F^- for a given species each consist of a number of terms depending on the other populations in the network. For the networks of primary interest to us in astrophysics the depletion flux for the population y will be proportional to y,

$$F^- = (k_1 + k_2 + \ldots k_n)y \equiv ky, \tag{4.4}$$

where the k_n are rate parameters (in units of time^{-1}) for each process that can deplete y (these may generally depend on the others populations y_i, and on system variables such as temperature or pressure).* From Eq. (4.4) we may define the effective depletion rate for the population y at a give time as as

$$k = \frac{F^-}{y}, \tag{4.5}$$

permitting Eq. (4.3) to be written as

$$y = \frac{1}{k}\left(F^+ - \frac{dy}{dt}\right). \tag{4.6}$$

Thus, in a finite-difference approximation at timestep t_n we have

$$y(t_n) = \frac{F^+(t_n)}{k(t_n)} - \frac{1}{k(t_n)}\left.\frac{dy}{dt}\right|_{t=t_n}. \tag{4.7}$$

We now define the *asymptotic limit* to be $F^+ \simeq F^-$, implying that $dy/dt \simeq 0$. In this limit Eq. (4.7) then gives as a first approximation for $y(t_n)$

$$y^{(1)}(t_n) = \frac{F^+(t_n)}{k(t_n)}. \tag{4.8}$$

*For 3-body reactions like triple-α the effective k itself will also depend on the population y.

For small dy/dt we may then get a correction term by using $y^{(1)}(t_n)$ from Eq. (4.8) to approximate the derivative term in Eq. (4.7)

$$\left.\frac{dy}{dt}\right|_{t=t_n} \simeq \frac{1}{\Delta t}\left(y_n^{(1)} - y_{n-1}^{(1)}\right) = \frac{1}{\Delta t}\left(\frac{F^+(t_n)}{k(t_n)} - \frac{F^+(t_{n-1})}{k(t_{n-1})}\right). \tag{4.9}$$

Therefore, Eq. (4.8) is improved to

$$y_n^{(2)} \simeq \frac{F_n^+}{k_n} - \frac{1}{k\Delta t}\left(\frac{F_n^+}{k_n} - \frac{F_{n-1}^+}{k_{n-1}}\right), \tag{4.10}$$

where we now employ compact index notation $y_n \equiv y(t_n)$, and so on. Because we are approximating the derivative term defined in Eq. (4.7) at time t_n by its average between t_n and t_{n-1}, we expect that Eq. (4.10) is valid only if the second term is small, implying that our asymptotic approximation becomes more valid if $k\Delta t$ is large.

4.3.5 Asymptotic Flux-Constrained Algorithm

We now use the preceding to define an explicit asymptotic flux-constrained integration algorithm: At each timestep, cycle through all network populations and compute the product $k_i\Delta t$ for each species i using Eq. (4.5) and the proposed timestep Δt. Since formally we expect an explicit integration to be stable if $k_i\Delta t < \kappa$ and to potentially be unstable if $k_i\Delta t \geq \kappa$, where κ is a number of order one, for each population species i

1. If $k_i\Delta t < 1$, update the population using the flux-constrained explicit algorithm.

2. Otherwise, update the population using the asymptotic approximation given in Eq. (4.10).

Notice that at each timestep some species may be updated by the flux-constrained explicit approach and some by the asymptotic approximation, and that the division of species between these two categories may change at each timestep since the product $k_i\Delta t$ may change at each timestep for each species. Also, the approximation (4.10) does not guarantee that total population is exactly conserved, so in setting an adaptive timestep one should make a check that ensures conservation of population at the level required by the problem at hand. Generally, if population conservation does not satisfy the required tolerance at a given timestep, making the timestep smaller will tend to

improve conservation of population because it will reduce $k_i \Delta t$ and therefore will tend to decrease the number of isotopes being treated asymptotically.

In the next section we demonstrate the dependence of results in the asymptotic approximation on conservation of population and demonstrate that for precise enough conservation of population the asymptotic approximation gives results essentially identical to results from exact numerical integration.

Chapter 5

Tests of Explicit Methods on Alpha Networks and under Hot CNO Conditions

In the previous chapter a new approach to providing stability for time integration of complex networks was discussed. Curing stiffness requires different medicine depending on whether you are far from or approaching nuclear statistical equilibrium (NSE). Tests of the validity of the method are performed in this chapter for two cases of significance in astrophysics: alpha networks and hot CNO (nova explosion) conditions. The computational examples presented here demonstrate the high accuracy and efficiency of the new method both in the areas that are far from and those that are approaching NSE. The influence of the tolerance parameter associated with imposing mass (particle-number) conservation on the accuracy is also demonstrated.

5.1 Energy and Isotope Production in an Alpha Network

Figures 5.1 and 5.2 illustrate a comparison of energy production rate dE/dt and integrated energy production E as a function of time (in seconds) for an alpha network integrated to NSE. The exact results are from an explicit integration with short enough timestep to be stable. The other cases correspond to asymptotic approximations with different choices for the tolerance parameter, which is the deviation of sum of mass fractions from 1.0 (it is called masTol in Figs. 5.3 and 5.4) that limits

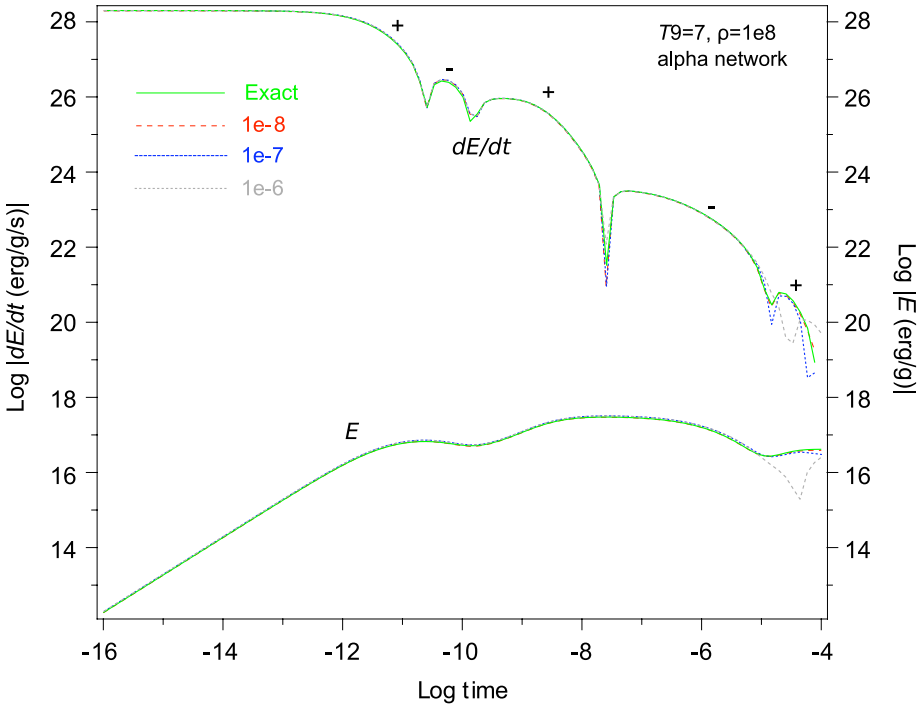

Figure 5.1: Energy production rate dE/dt and integrated energy production E for various levels of asymptotic approximation compared with an exact numerical integration. The asymptotic curves are labeled by the value of the tolerance parameter defining the maximum fractional violation of particle number permitted in a single integration step. These calculations used an alpha network with REACLIB reaction rates at constant temperature $T = 7 \times 10^9$ K and constant density $\rho = 1 \times 10^8$ g cm^{-3}. For tolerance parameters of 10^{-8} or smaller the asymptotic result is essentially exact over the entire integration range (compare the red dashed curve with the green solid curve).

the maximum violation of particle number that can occur in one integration step. Note that in Fig. 5.1 a tolerance of 1×10^{-8} gives essentially exact results over the entire range of integration (the dashed red line), while larger values of this parameter give essentially correct results at larger energy production but increasingly deviate from the correct result at late times (low energy generation rate). Since E and dE are plotted on log scales, the absolute value is plotted and $+$, $-$ is used to denote the sign for dE/dt, which fluctuates between positive and negative in this calculation. Likewise, in Fig. 5.2 the asymptotic result is indistinguishable from the exact result over the entire time range for small tolerance parameters.

Figures 5.3 and 5.4 illustrate a comparison of mass fractions as a function of time for an alpha network integrated to NSE. The exact result is from an explicit integration with short enough timestep to be stable. The other cases correspond to asymptotic approximation with different

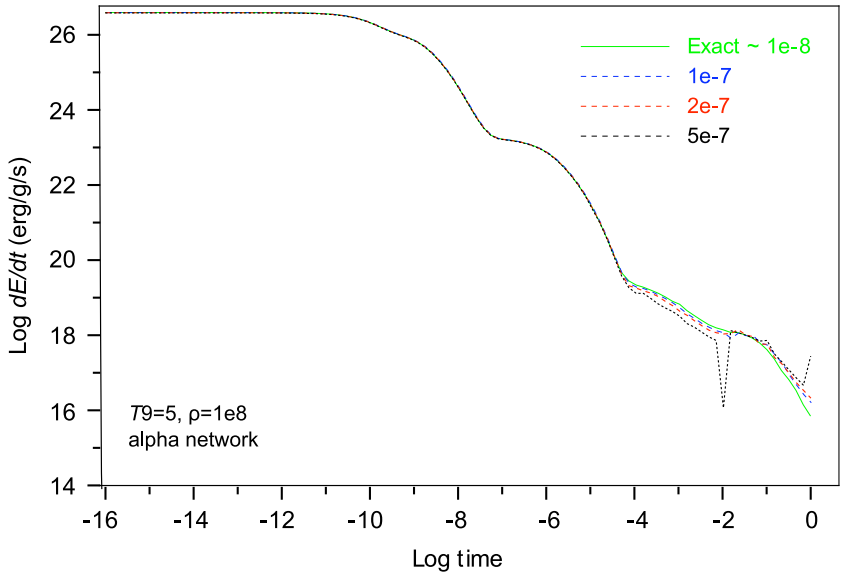

Figure 5.2: Rate of energy production dE/dt as in Fig. 5.1 but for constant $T = 5 \times 10^9$ K and constant $\rho = 1 \times 10^8$ g cm^{-3}. For tolerance parameters of 10^{-8} or smaller the asymptotic result is indistinguishable from the exact result (green line) over the entire integration range, and the more generous tolerance parameters cause deviations only at the very latest times.

choices for the parameter that limits the maximum violation of particle number that can occur in one integration step. Note from Fig. 5.4 that a tolerance of 1×10^{-8} gives essentially exact results over the entire range of integration while a tolerance of 1×10^{-6} gives almost exact results except for small differences at late times (Fig. 5.3).

5.2 Hot CNO Cycle at Constant Temperature and Density

Some isotopic abundances under nova (hot CNO) conditions calculated using the explicit asymptotic algorithm are shown in Fig. 5.5 (these are representative; of order 100 isotopes are populated in the calculation). The rates are strongly temperature and density dependent, and were recomputed at each timestep in the algorithm (the computation of such rates is typically the most time-consuming step of a realistic explicit calculation). However, for simplicity in comparison here a constant temperature and density time profile was assumed, with a temperature of 0.25×10^9 K and a density of 500 g cm^{-3}. In this and subsequent figures illustrating calculations under nova conditions, an initial isotopic abundance distribution enriched in heavy elements has been assumed and reaction

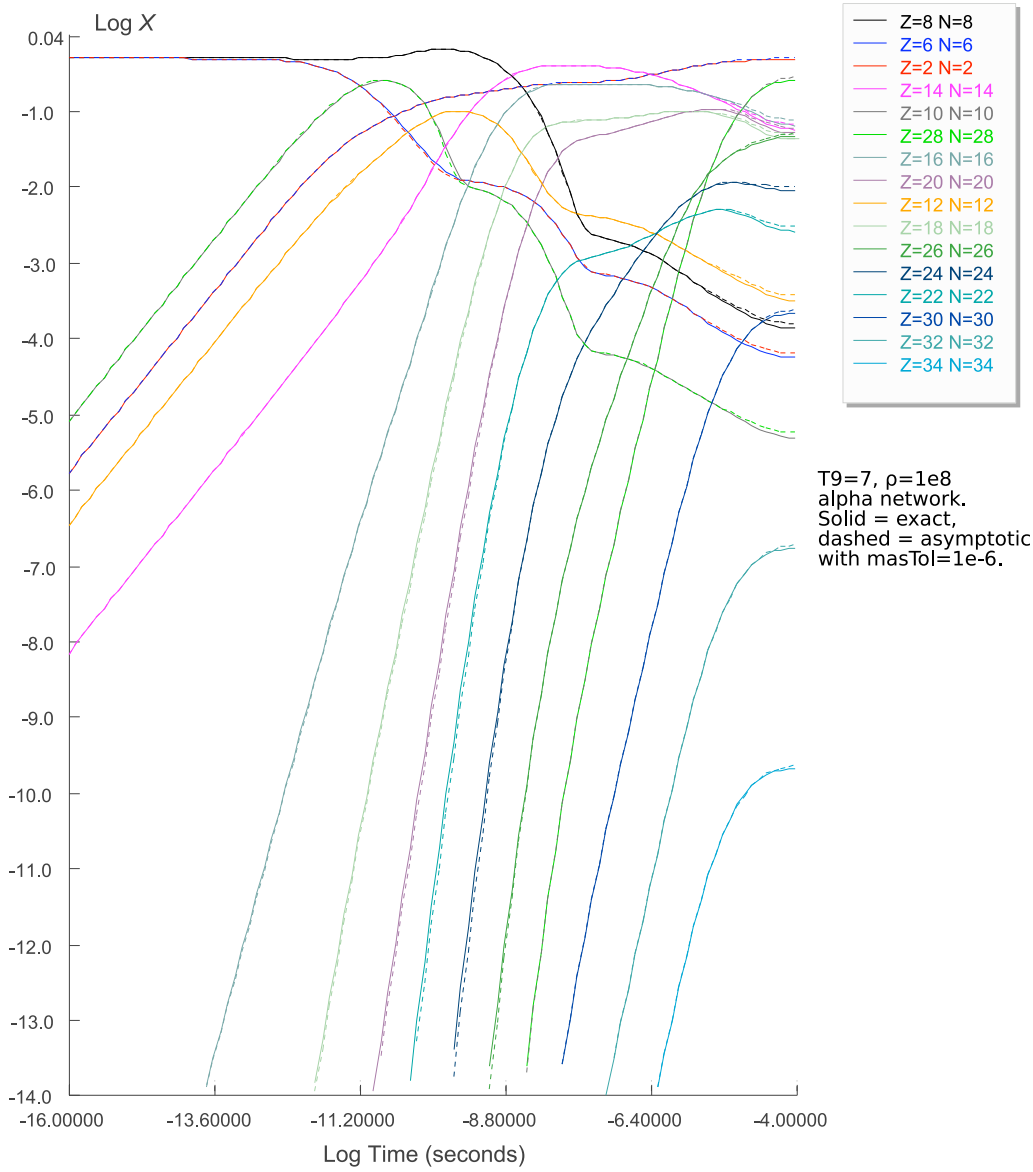

Figure 5.3: Comparison of mass fractions X for isotopes in the alpha network of Fig. 5.1. Solid lines represent exact numerical integration and dashed lines illustrate an asymptotic approximation with a particle number conservation tolerance number of 1×10^{-6}. The asymptotic and exact results are indistinguishable except for small differences at very late times. Compare with Fig. 5.4, where the asymptotic result is essentially exact over the entire time range.

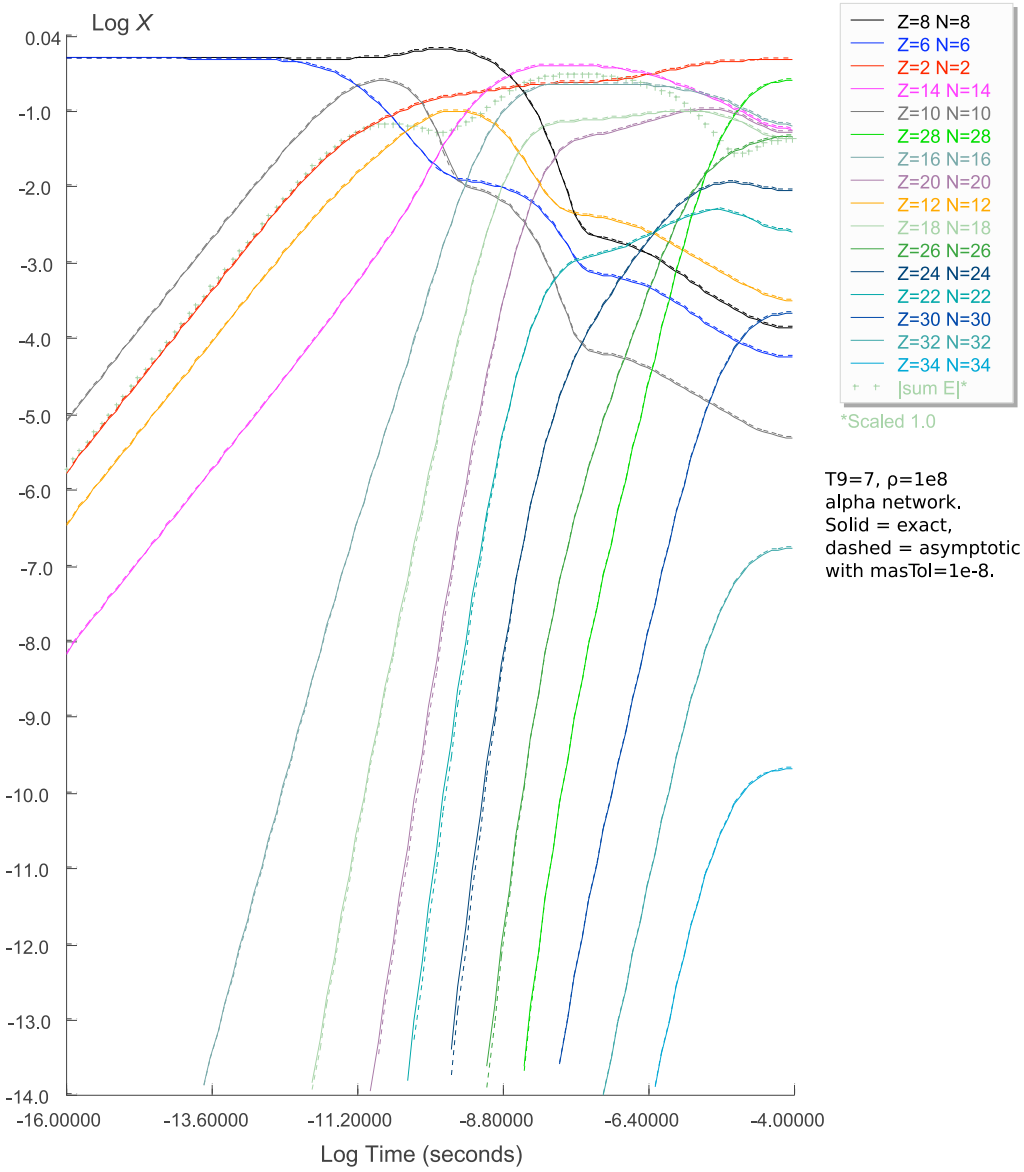

Figure 5.4: Comparison of mass fraction X for isotopes in the alpha network of Fig. 5.1. Solid lines represent exact numerical integration and dashed lines illustrate an asymptotic approximation with a particle number conservation tolerance number of 1×10^{-8}. For this value of the tolerance parameter or smaller, the asymptotic results are indistinguishable from the exact result. The integrated energy production is also illustrated by green $+$ symbols and is indistinguishable between the exact and asymptotic approximations.

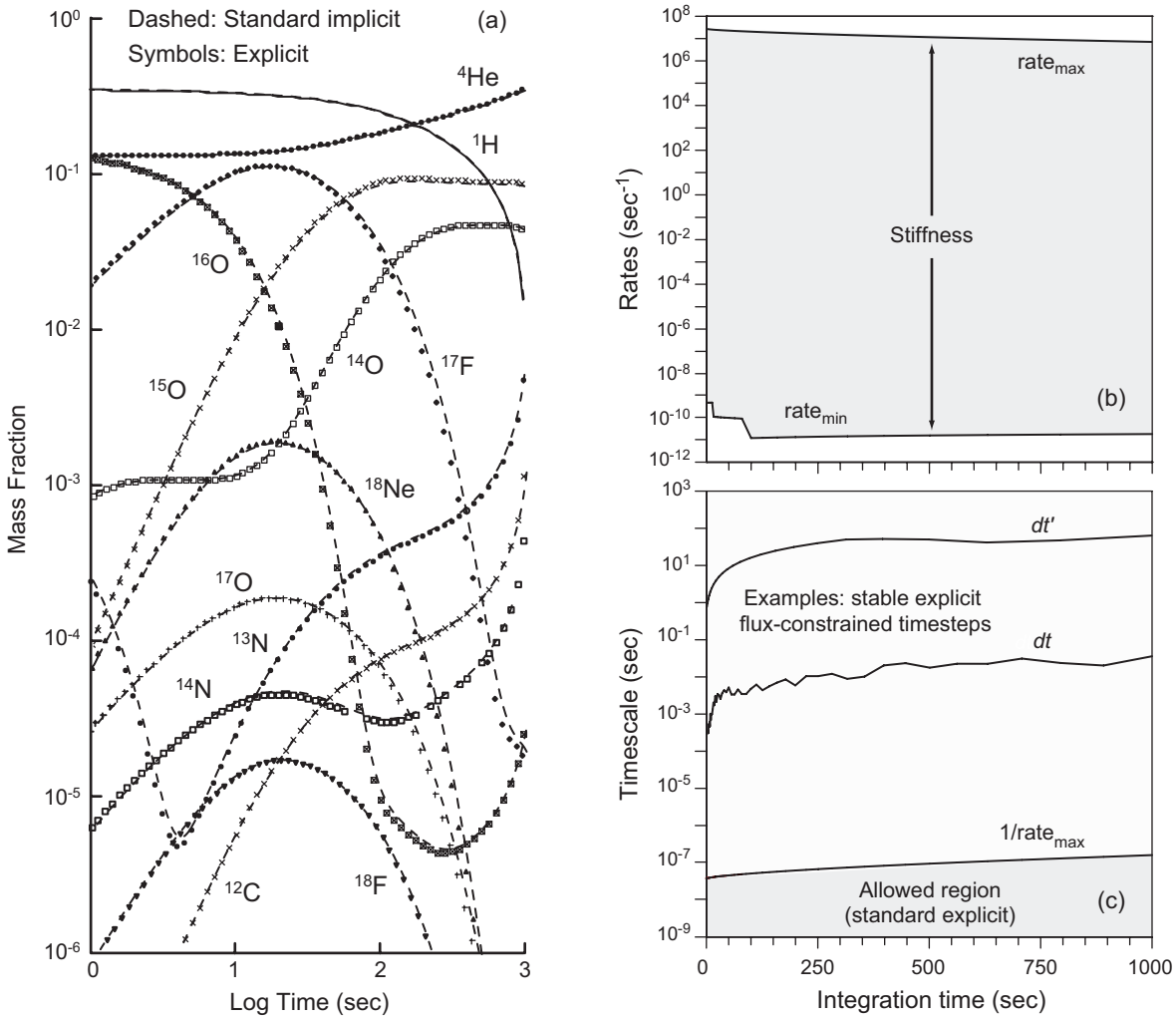

Figure 5.5: (a) Arbitrarily selected isotopic abundances under nova (hot CNO) conditions calculated using the flux-constrained explicit algorithm. For this test case the temperature was $T_9 = 0.25$ and the density was 500 g cm^{-3}. Representative mass fractions were selected arbitrarily and compared with an implicit integration. The network contained 145 isotopes, with 924 non-zero couplings. (b) Rates and timescales characteristic of a nova simulation. Conditions as for part (a) but with a larger reaction library: 896 isotopes with 8260 couplings were included but the algorithm traverses only the non-zero flux links in any timestep. Extremal rates plotted are restricted to those involving non-zero fluxes. (c) Comparison of maximum stable timestep [$\simeq 1/\text{rate}_{\max}$ from part (b)] possible for a standard explicit integration with much larger stable timesteps dt and dt' for some representative explicit flux-constrained integrations.

rates from the REACLIB library [33] have been used. Figure 5.5(a) (a) displays some representative populations, with the results of a standard implicit calculation [34] shown as dashed lines and the explicit flux-constrained calculations as symbols. Note the almost perfect agreement between implicit and explicit methods over six orders of magnitude in the mass fractions in Fig. 5.5(a). An adaptive timestep was used in the explicit integration, with the timestep adjusted to keep the number of particles transferred in a timestep for some key populations within a prescribed range. As we discuss further below, this timestep is *much* larger than would be stable in a standard explicit integration.

In the nova simulation the difference between the slowest and fastest rates is about 18 orders of magnitude at any timestep, as illustrated in Fig. 5.5(b). It is obvious that we deal with an extremely stiff system. If standard explicit algorithms are used, the largest timestep permitted is close to the inverse of the fastest rate in the network (see Ch. 16 of Ref. [30]). For the data presented in Fig. 5.5(b) the inverse of the fastest rate gives the lower curve in Fig. 5.5(c). Thus, stability requirements for a normal explicit algorithm will restrict timesteps by requiring them to be in the shaded region below this curve ($dt \simeq 10^{-7}$ seconds or less).

On the other hand for the flux-constrained explicit integration two curves, shown in Fig 5.5(c) and representing timesteps (adaptive), lie far above this region. The timestep for the curve marked dt is small enough to provide accuracy comparable to Fig. 5.5(a). At the same time it is about a factor of 10^5 larger than the one required to guarantee stability for a normal explicit integration. A much larger explicit algorithm timestep corresponding to the curve marked dt' compromises accuracy for weaker transitions, but stability is not lost and stronger transitions are computed correctly. The timestep $dt' \sim 100$ seconds is about 9 orders of magnitude larger that than would be stable for a standard explicit algorithm. Taking into account that dt' already is comparable to the characteristic timescale ($\sim 10^3$ seconds) of the entire physical process being simulated, it is clear from this example that a stable explicit flux-constrained integration timestep can in some cases be effectively arbitrarily large in comparison with the usual upper limit for explicit methods.

5.3 Large Networks under Nova Conditions

In the last two figures of this chapter a network under nova conditions is considered. Figure 5.6 illustrates evolution of a thermonuclear network with a hydrodynamic temperature–density profile taken from simulations of hot nova outbursts. Figure 5.7 illustrates the hydrodynamic profiles and other conditions associated with the calculation in Fig. 5.6.

In the calculations the hydrodynamic profiles represent temperature and density as a function of logarithm of time (computed from hydrodynamical simulations). They are depicted on the bottom right of Fig. 5.6 (the profiles are reproduced for convenience in Fig. 5.7 also on the right side). The analysis starts where heavier elements are quite abundant. On the top of Fig. 5.6 mass fractions and released integrated energy are plotted vs. logarithm of time. The results of the calculations—isotopic abundance patterns—are presented on the bottom of this figure from the left side in the proton vs. neutron plane. Note again from Fig. 5.7 that the asymptotic explicit timestep is much larger (6-8 orders of magnitude) than would be possible for a normal explicit method. This entire calculation is so fast that it is difficult to time, completing in a fraction of a second on a modern processor.

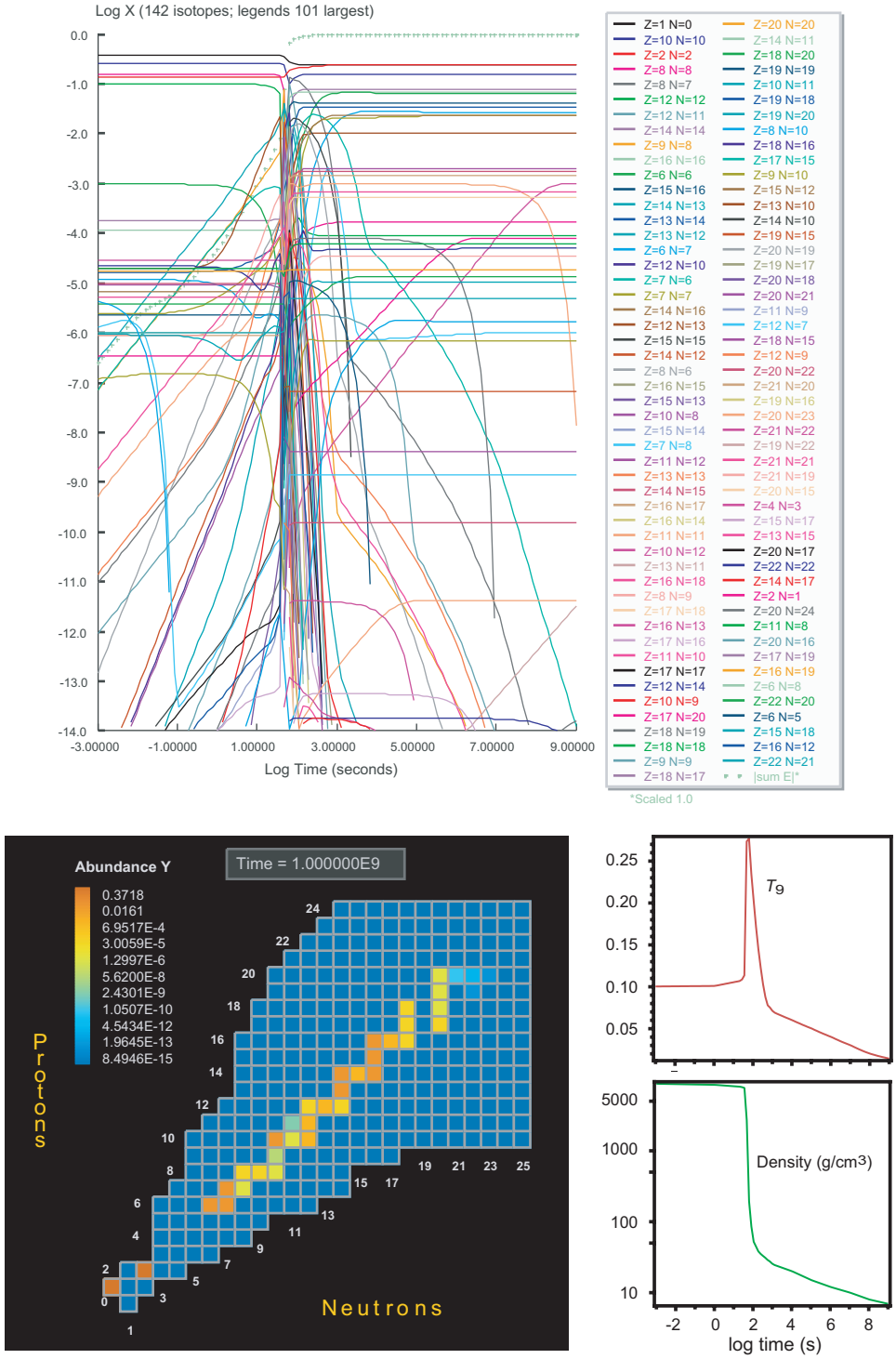

Figure 5.6: Evolution of a network under hot nova conditions starting with an enriched abundance of heavier elements. The top figure shows the evolution of individual mass fractions and the integrated energy release (plus signs). The bottom left figure shows the isotopic abundance pattern at the end of the simulation. The bottom right figure shows the temperature and density hydrodynamic profiles assumed in the calculation. Additional details of the simulation are shown in Fig. 5.7.

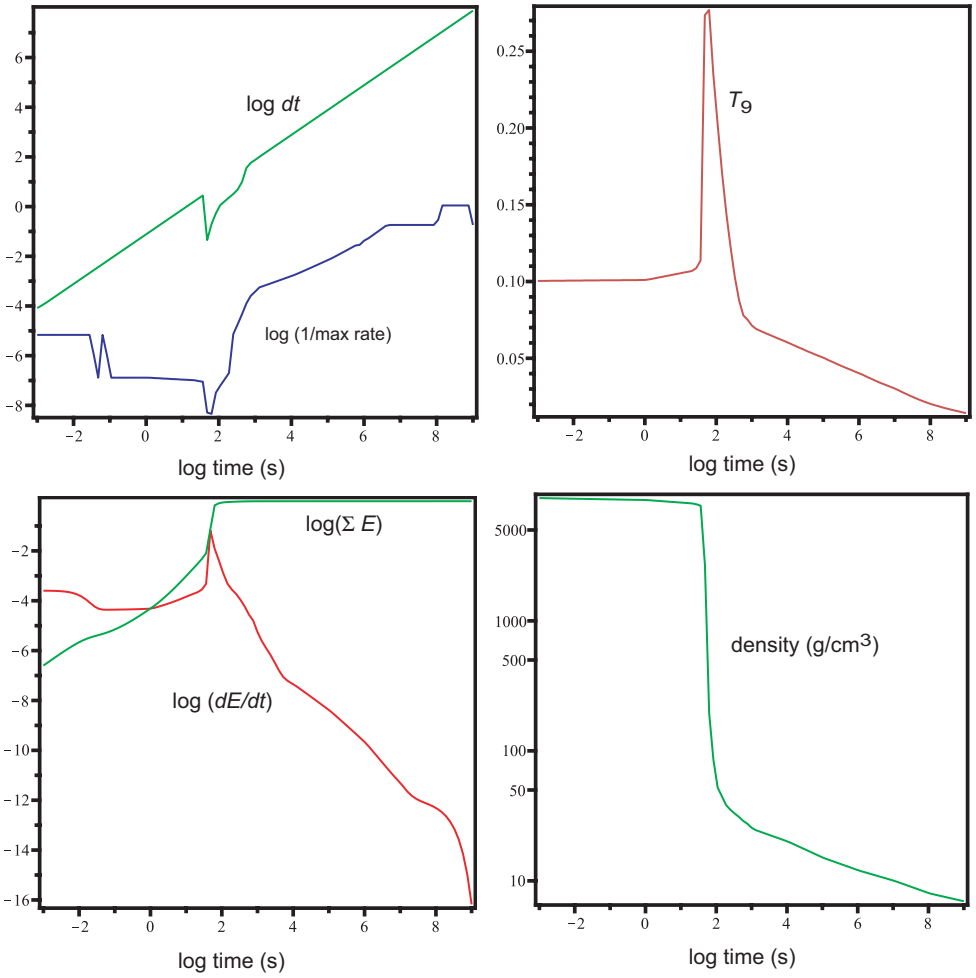

Figure 5.7: Hydrodynamic profiles and other conditions associated with the calculation in Fig. 5.6. The energy units are MeV/nucleon and the units of dE/dt are Mev/nucleon/second. The network integration stepsize is dt and the inverse of the maximum rate in the network is a general measure of the largest integration step that would be stable using a standard explicit method. The flux-limited asymptotic explicit method employed here is seen to permit stable timesteps that are 6-8 orders of magnitude larger than would be permitted for a normal explicit method in this example.

Chapter 6

Post-Processing Tests of Explicit Methods under Type Ia Conditions

In the previous chapters we analyzed the example of running networks using hydrodynamics profiles. Now it is time to consider this question in a more detailed manner for the specific problem of Type Ia supernovae.

6.1 Post-Processing Approximations

In astrophysics often a procedure called post-processing is used. In application to our case, post-processing simply means that initially a small network is coupled to hydrodynamics. The temperature and density profiles that are obtained in this case are then used to solve the full network problem. It is clear that such an approach is not entirely correct. But since coupling a full network to hydrodynamics has been very difficult in the past, using the profiles obtained after running hydrodynamics coupled to a small network can give a feeling for the physics of what could possibly happen if a full network would be coupled to hydrodynamics. It is obvious that this approach is far from rigorous from the point of view of mathematics but its usefulness, especially under some known physical conditions, can be understood and justified.

6.2 Example: High-Density, High-Temperature Burns to NSE

The energy released in a Type Ia supernova explosion derives primarily from the thermonuclear burning of carbon and oxygen to heavier nuclei. If the explosion lasts long enough to achieve nuclear statistical equilibrium (NSE), the primary final products of this burning will be iron-group nuclei (unless the temperature becomes so high that all nuclei photodisintegrate into alpha particles). An example of network evolution under conditions typical of the Type Ia explosion in the deep interior of the white dwarf is illustrated in Fig. 6.1.

In this calculation, the initial temperature was $T_9 = 2$, the initial density was $\rho = 1 \times 10^8$ g cm^{-3}, and the initial composition was assumed to be equal mass fractions of ^{12}C and ^{16}O. The explosion is initiated by carbon burning, which quickly raises the temperature (see the inset to the figure) and initiates burning of oxygen and all the reaction products that are produced by carbon and oxygen burning. The rapid temperature rise is associated with the coupling of the large energy release from the thermonuclear burning described by the reaction network to the fluid of the white dwarf, which is described by hydrodynamics. This energy release (through the equation of state) causes a rapid rise in temperature in the fluid representing the white dwarf, and this in turn increases rapidly the rate of nuclear reactions in the network. The net result is the almost vertical rise in temperature from $T_9 \sim 2$ to $T_9 \sim 6.6$ in a period of less than 10^{-5} s, during which time the isotopic species in the network have increased from 2 to about 500, with significant population of the iron group of nuclei already evident (see the population distribution versus proton number and neutron number in the lower portion of Fig. 6.1). The very narrow range in time in Fig. 6.1 over which the network releases much of its energy and over which the temperature rises from $T_9 \sim 2$ to $T_9 \sim 6.6$ is illustrated in greatly expanded scale in Fig. 6.2. Notice the rapid increase in population for hundreds of new elements. Under these conditions, as the thermonuclear flame burns through the white dwarf the carbon and oxygen fuel in each region is burned in a tiny fraction of a second, and the entire white dwarf is consumed on a timescale of less than a second.

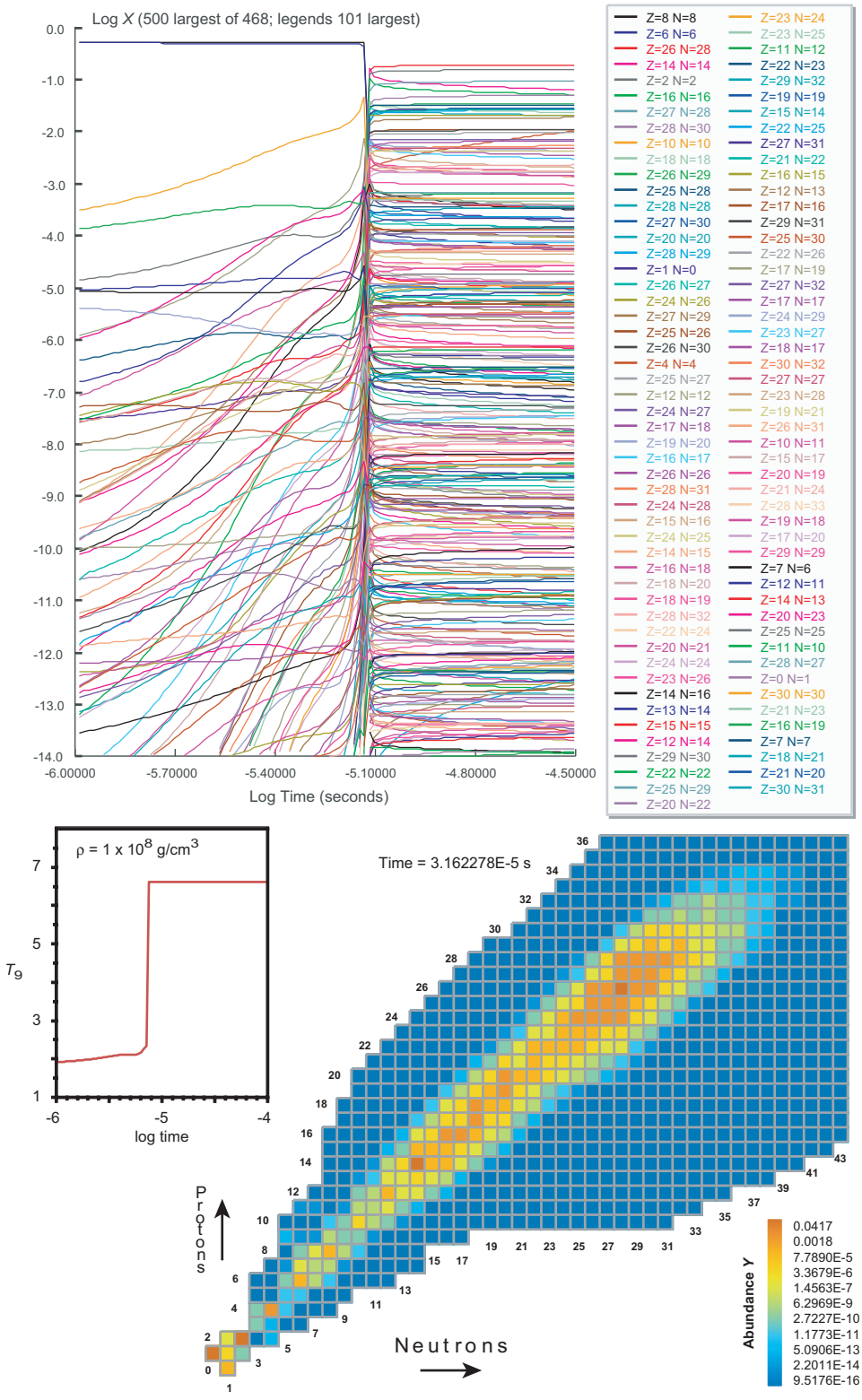

Figure 6.1: Element production in a Type Ia explosion. Upper: mass fractions X for 468 isotopes. Lower: distribution of abundances Y for all isotopes at end of calculation in the upper figure. Inset on left shows the variation of temperature with time (density remains almost constant over this time period).

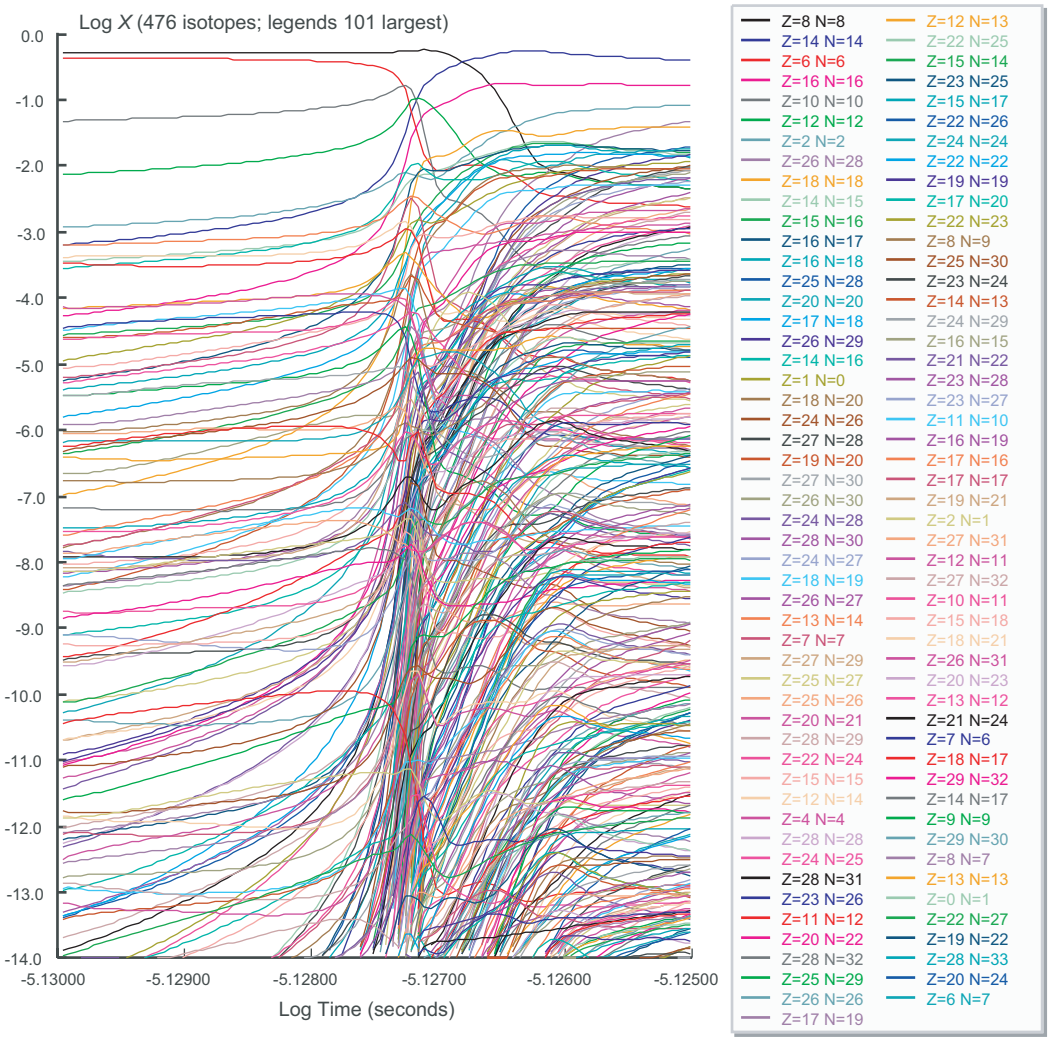

Figure 6.2: Calculation of Fig. 6.1 with the timescale greatly expanded in the region where much of the energy is released and there is a rapid increase in temperature.

6.3 Example: Gravity-Confined Detonation Conditions

Figure 2.5 illustrates the gravity confined detonation (GCD) mechanism which was discussed in Section 2.5 earlier. The profile is given by the insert in the bottom picture of Fig. 6.3. While analyzing the evolution of abundances under these conditions, what impresses first of all is that the processes are extremely fast, especially if one takes into account that the events are happening in a very large body. The major nuclear transformations, as it follows from the top picture of Fig. 6.3, are basically concentrated around the beginning of NSE and covering a small fraction of the x-axis, which itself spans a tiny time interval. The results of computations (final abundances) after running the network are presented in the bottom part of Fig. 6.3. A broad spectrum of isotopes is shown on this figure. Just a tiny fraction of a second ago there were only two elements present. This idea of extremely fast processes and intense interaction of isotopes producing the new ones is demonstrated in more detail in Fig. 6.4. A sequence of snapshots of abundances in the proton vs. neutron plane is depicted here. It is easy to see how the new isotopes are born and how their abundances are changing with time from this sequence.

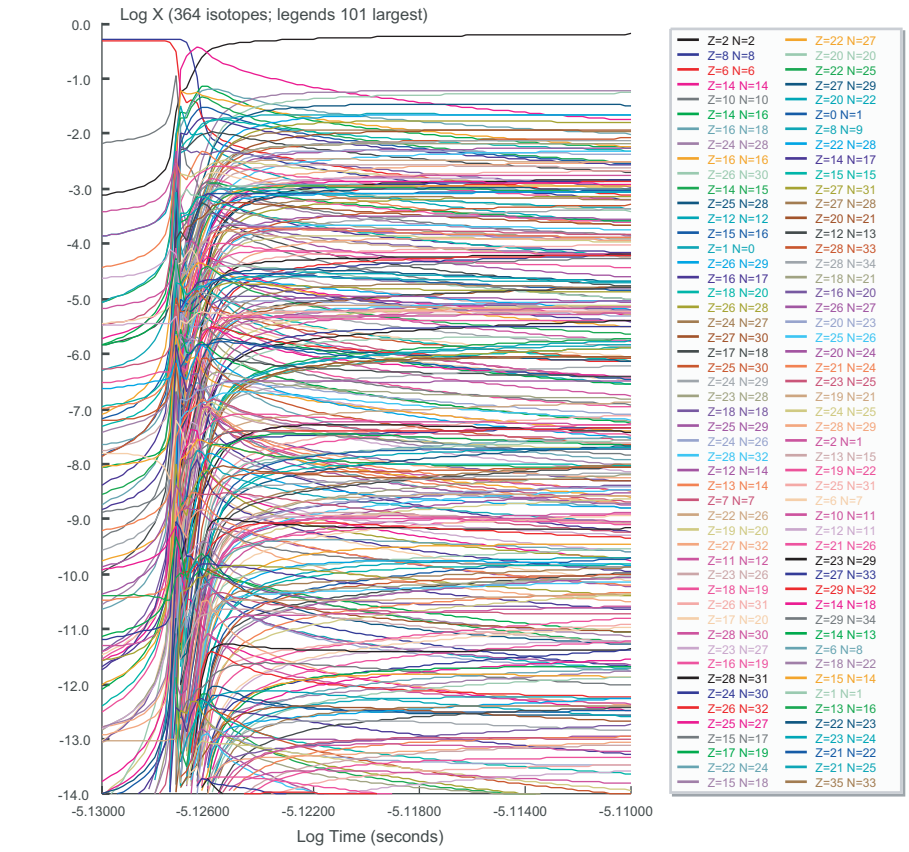

Figure 6.3: Mass fractions (top) and abundances (bottom) for a temperature profile (lower right) thought to be characteristic of gravity confined detonation conditions. The evolution of abundances with time in this calculation is illustrated further in Fig. 6.4.

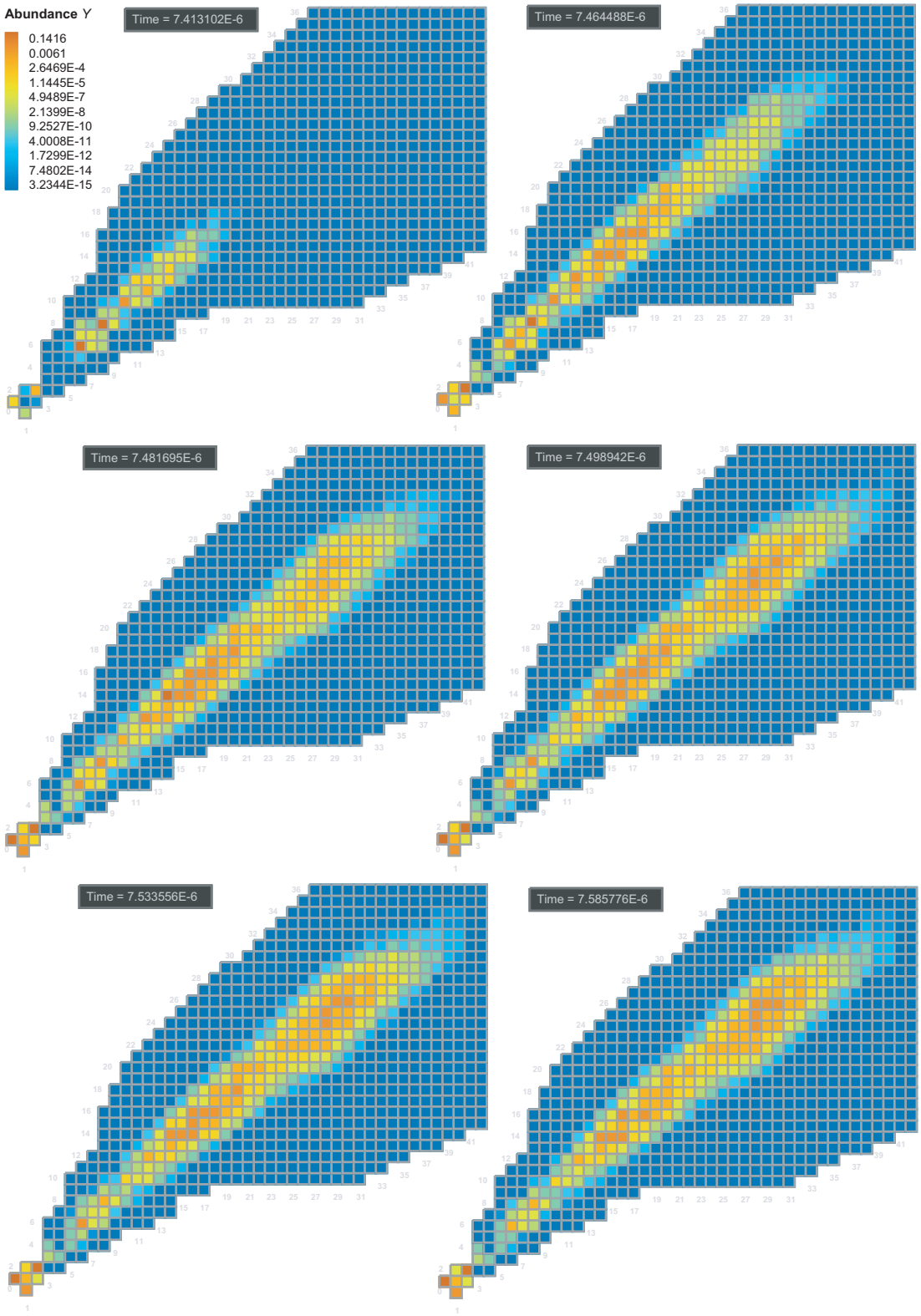

Figure 6.4: Evolution of abundances in the proton (vertical) and neutron (horizontal) plane as a function of time for the calculation presented in Fig. 6.3.

Chapter 7

Operator-Split Coupling of Realistic Networks to Hydrodynamics for the Type Ia Supernova Problem

In this section we finally come to the heart of the matter and demonstrate the coupling of a realistic network to 3-dimensional radiation hydrodynamics under conditions expected in Type Ia supernovae. We have run various simulations recently suggesting that large networks coupled to 3-dimensional hydrodynamics using the explicit flux-limited asymptotic methods described in previous chapters may now represent a tractable numerical problem. We shall illustrate with one example below, and will discuss the results of calculations below.

Figure 7.1 illustrates a calculation using a 150-isotope network and the FLASH 3D hydrodynamics code, with the network coupled to the hydrodynamics by operator splitting. In this simulation the initial conditions were $T = 3 \times 10^9$ K and $\rho = 1 \times 10^7$ g cm^{-3}, with initial equal mass fractions of ^{12}C and ^{16}O. These conditions were chosen because they are are thought to be similar to those that may prevail at the onset of the gravity confined detonation (GCD) mechanism discussed in previous chapters. The variation of the energy production rate and the temperature for this simulation are shown in Fig 7.2.

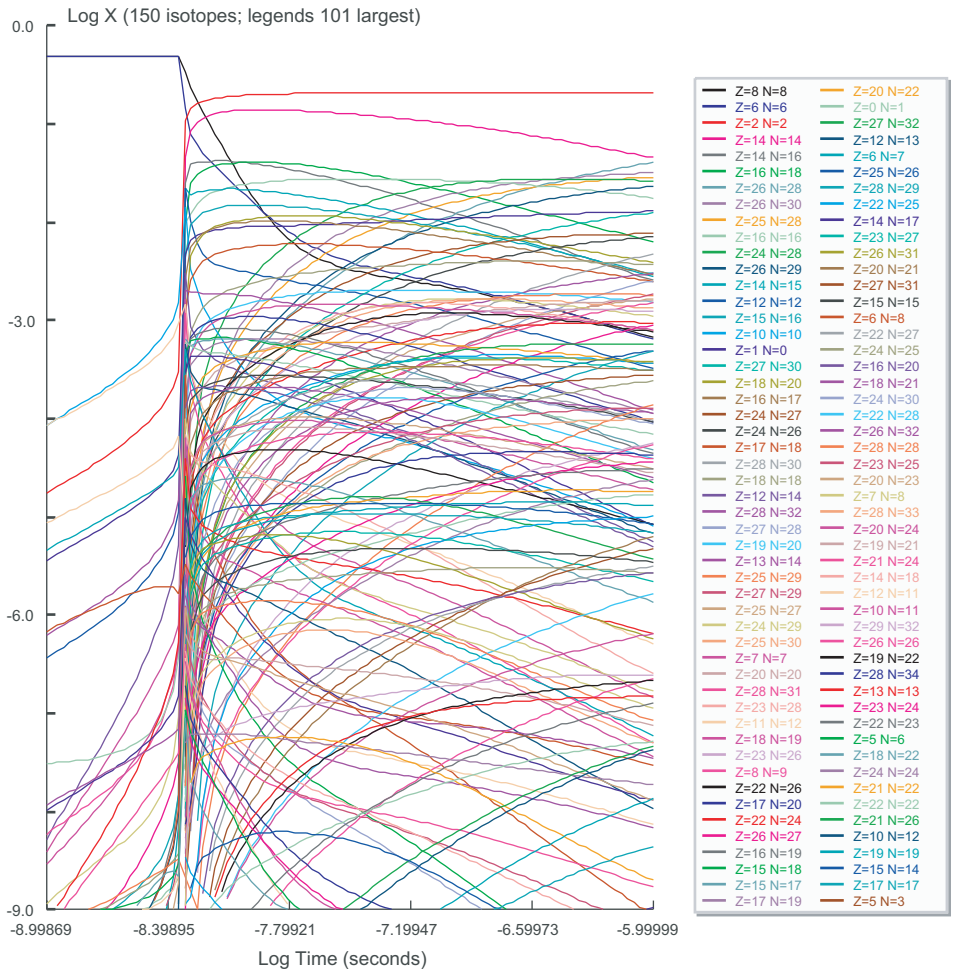

Figure 7.1: A 3-dimensional hydrodynamics simulation coupled to a realistic network.

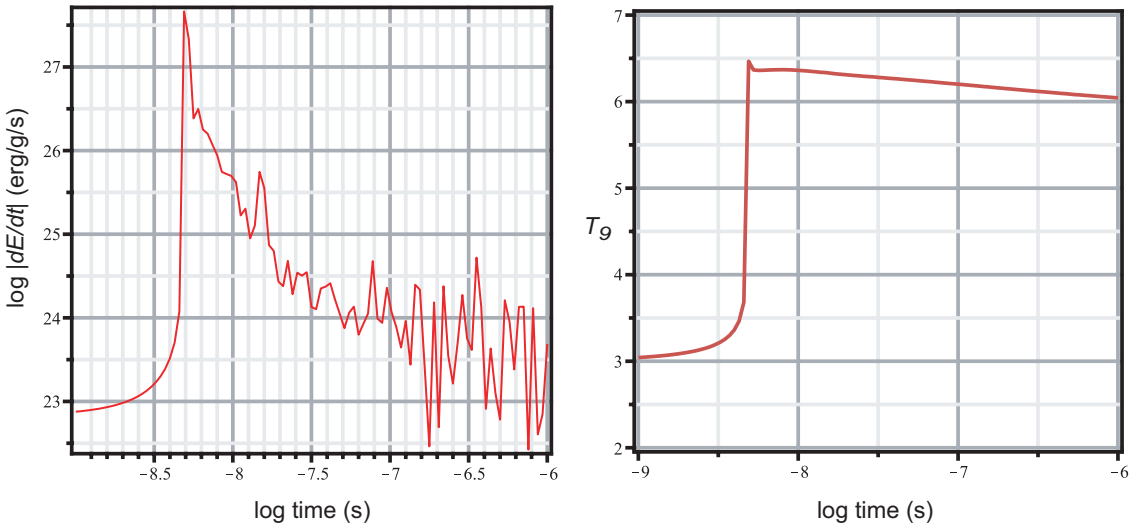

Figure 7.2: Variation of the temperature and energy production rate with time for the calculation illustrated in Fig. 7.1. Over this time range, the density of the system remains essentially constant at its initial value.

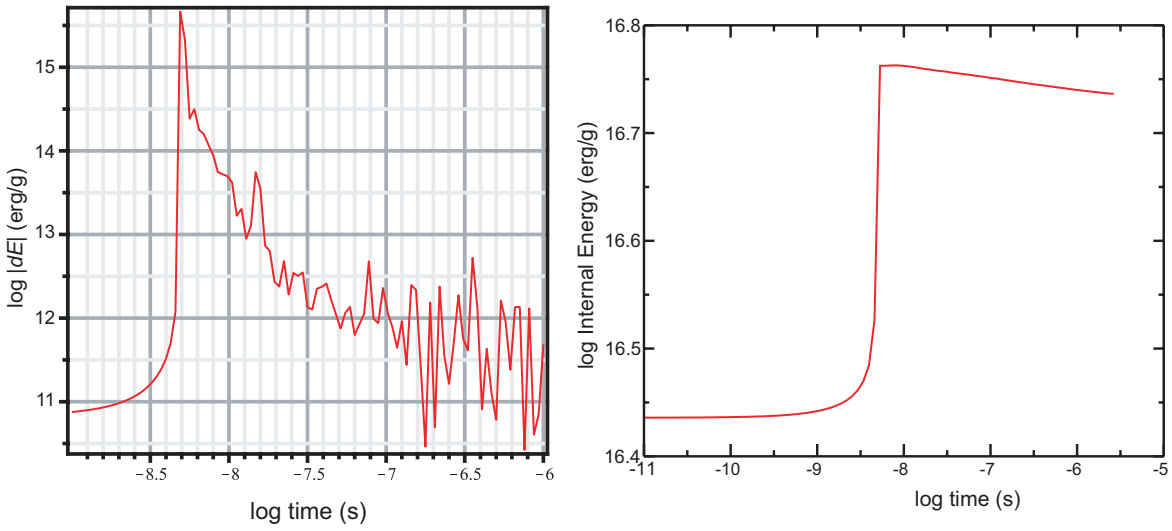

Figure 7.3: Comparison of average energy released by the network per hydrodynamic timestep $dE = (dE/dt)dt$ with the internal specific energy of the gas as a function of time. The left figure was constructed from the left figure in Fig. 7.2 by multiplying by an average timestep. The fluctuations in dE at late times are seen to be many ofders of magnitudes smaller than the specific energy of the gas at that time.

These figures represent a snapshot of an ongoing calculation after approximately 13 hours of running on a single 2 GHz P4 processor. The rapid burning of the carbon and then the oxygen produces a large outpouring of energy (see Fig. 7.3) that quickly raises the temperature to $T \sim 6.5 \times 10^9$ K (under these conditions the density remains essentially constant over the time ranges simulated here). By the end of the snapshot shown here the system is well on its way to nuclear statistical equilibrium: the alpha particles are already the dominant species and are nearly equilibrated, and most of the silicon group has already burned to iron-group nuclei (with various iron-group nuclei such as ^{54}Fe already approximately equal to ^{28}Si in mass fraction), and the net rate of energy production is decreasing rapidly and is already down by 4 orders of magnitude from its peak, though it is exhibiting large fluctuations at lower energy production rates that need to be understood.

The energy fluctuations described in the preceding paragraph appear to be associated with a bug in the network timestepping algorithm that causes it intermittently to take a timestep too large to resolve fully the energy release at lower energy production rates. Tests with the network uncoupled from the hydrodynamics indicate that a too-aggressive timestep can cause such an energy fluctuation, and we have shown that the timestepper in the code coupled to FLASH is sometimes taking a too-aggressive timestep that is not taken by the reference version of the code (which is written in Java rather than F90). Work is underway to correct this problem. However, although the energy release is fluctuating at later times, we note that there is little evidence that this is causing a corresponding fluctuation in other quantities like the temperature, internal energy, or the elemental abundances. This can be understood in basic terms. Near maximum energy production from the network (carbon and oxygen burning), for the timesteps being taken by the hydrodynamic solver the energy released in a single hydrodynamical timestep is a significant fraction (0.001–0.01) of the specific internal energy of the gas. However in the region exhibiting fluctuations in Fig. 7.2, the energy being released per unit mass per hydrodynamical timestep by the network is many orders of magnitude smaller than the internal energy per unit mass of the gas. Thus the fluctuations in Fig. 7.2 are not of much practical consequence and do not alter the hydrodynamical evolution significantly, leaving quantities like the temperature, internal energy and the elemental abundances undisturbed.

The bulk of the mass has been burned to the iron group and light ions by the latest time shown from this ongoing calculation, but notice that there is appreciable population distributed over a broad range of isotopes between silicon and iron that looks as if it will remain until the end of the explosion

since the system is beginning to equilibrate. This is important because of the earlier discussion that observations require a substantial amount of intermediate-mass material to be produced in the Type Ia explosion, and that the GCD mechanism is one promising idea to cause part of the white dwarf to be consumed in a deflagration and part in a detonation that could in combination produce the required mix of elements in the explosion debris.

Initial tests with larger networks coupled to the hydrodynamics code suggest that the time to run the network does indeed increase approximately linearly with the size of the network, as expected on conceptual grounds for the explicit asymptotic algorithm. Therefore, it appears that the coupling to multidimensional hydrodynamics of even larger networks than that shown here may be feasible using this technique. Initial simulations with larger networks are underway.

Chapter 8

Summary and Conclusions

It is important in any doctoral dissertation to state clearly what has been accomplished and why this represents a significant advance, what remains to be done to consolidate and exploit this advance, and what promising new directions are suggested by the thesis work.

8.1 What Has Been Accomplished in this Work

- A new method has been applied to solving large thermonuclear networks, and has been demonstrated to do a good job for a number of applications of importance in astrophysics.
- Much work remains to be done, but for the first time a network that can be called "large" by modern standards has been implemented in the reactive hydrodynamics code FLASH and the resulting simulations have been shown to be tractable, if challenging, for reasonable resolutions and processor counts under Type Ia supernova conditions. Thus, coupling of networks of realistic size to state-of-the-art multidimensional hydrodynamics codes shows considerable promise, based on the results obtained to this point.
- The linear scaling expected for the explicit methods that we have tested has been demonstrated to occur under realistic conditions in networks of astrophysical interest. This holds considerable promise for future work with even larger networks since, in contrast to the case for the cubic scaling of standard implicit codes, significant increases in network size do not cost much computationally with this approach.

- A state-of-the-art code such as FLASH can now incorporate much more realistic physics in supernova simulations. Initial comparisons of calculations with small networks and networks of realistic size suggest that the results for them can differ quite noticeably. This is not surprising. For example, the realistic networks used in the present study include proton and neutron reactions that are completely absent from the networks used in standard supernova simulations. The potential significance of this follows immediately upon noting that the fastest reactions under supernova conditions are often proton or neutron reactions, not alpha network reactions.

8.2 What Remains to Be Done

The results presented in this dissertation demonstrated that the flux-constrained asymptotic method itself, and its coupling with FLASH, were efficient and promising. However, the testing demonstrated here has been implemented using versions of the flux-constrained asymptotic approach that are far from optimized numerically, and that have yet to incorporate into the algorithm improvements that have already been demonstrated in test applications to greatly increase the speed of the code. Our testing suggests that deployment of these demonstrated algorithmic improvements, coupled with standard aggressive numerical optimization, can realize increases in speed over the present calculations by factors of 100 or more. Such development tasks are important for the eventual deployment of the approaches developed here for systematic large-scale simulations with realistic networks.

8.3 What New Directions Are Suggested by this Work

The flux-constrained asymptotic approach discussed here has permitted initial calculations with realistic networks coupled to 3-dimensional hydrodynamics. However, the asymptotic approximation that is critical to the speed of this approach works very efficiently through the carbon and oxygen burn (where most of the energy is released), but it does not work nearly as efficiently in the approach to nuclear statistical equilibrium. Although the present work suggests that even with these limitations the current algorithm is fast enough for many realistic applications coupling large networks

to hydrodynamics, we believe that even greater speed and efficiency can be obtained by employing newer approaches specifically designed for the approach to nuclear statistical equilibrium. One such approach that is suggested by this work is a different approximation near equilibrium that exploits steady flux conditions there to damp stiffness instabilities for explicit timesteps. Another is suggested by work already initiated by Parete–Koon, Hix, and collaborators that takes advantage of quasi-equilibrium to reduce the effective number of isotopes in the network. (This latter approach would not help the present explicit approach so much by reducing network size directly because of the linear scaling, but it potentially could help a much larger amount through removing sources of stiffness, thereby permitting larger stable timesteps.)

With the above caveat in mind, however, it should be noted that the inclusion of a realistic network in Type Ia simulations is most important for realistic isotopic evolution in the distributed burning regime, i.e. at lower densities near the surface of the white dwarf. The time scale to achieve NSE at these densities ($\approx 1.0 \times 10^7$ g cm^{-3}) exceeds the explosion timescale (i.e. > 2 s). Therefore, it can be argued that the ability of a network solver to accurately characterize the isotopic evolution for burning stages up to silicon burning under these conditions is the most important criterion for utility. This requirement is already very close to being met in this work.

Bibliography

Bibliography

[1] W. Hillebrandt and J.C. Niemeyer, Annu. Rev. Astron. Astrophys. 2000. **38**: 191–230

[2] B. Leibundgut, Annu. Rev. Astron. Astrophys. 2001. **39**: 67–90

[3] A.V. Fillipenko, Annu. Rev. Astron. Astrophys. 1997. **35**: 309–355

[4] W.D. Arnett. 1996. Supernovae and Nucleosynthesis. Princeton Univ. Press

[5] J.C. Niemeyer, J.W. Truran, eds. 1999. Type Ia Supernovae: Theory and Cosmology. Cambridge, UK: Cambridge Univ. Press

[6] M. Livio, N. Panagia, K. Sahu, eds. 2000. Supernovae and Gamma-Ray Bursts. Cambridge, UK: Cambridge Univ. Press

[7] P. Ruiz-Lapuente, R. Canal, J. Isern, eds. 1997. Thermonuclear Supernovae. Dordtecht, Ger.: Kluwer

[8] B. Leibundgut, Nuclear Physics, **A688:** 1c–8c, 2001

[9] B. Leibundgut, Computer Physics Communication **147** 459–464, 2002

[10] J.L. Torny. et al., The Astrophysical Journal, **594:** 1–24, 2003 September 1

[11] B. Leibundgut, Astrophysics and Space Science **290:** 29–41, 2004

[12] S. Blinnikov, E. Sorokina, Astrophysics and Space Science **290:** 13–28, 2004

[13] A.G. Riess, et al., The Astronomical Journal, **607:** 665–687, 2004 June 1

[14] P.A. Pinto, R.G. Eastman, The Astrophysical Journal, **530:** 744-756, 2000, February 20

[15] L. Iapichino, M. Bruggen, W. Hillebrandt, and J.C. Niemeyer, Astronomy and Astrophysics, **450:** 655–665, 2006

[16] T. Plewa, A.C. Calder, and D.Q. Lamb, The Astrophysical Journal, **612:** L37-L40, 2004, Septermber 1

[17] M.M. Phillips, The Astrophysical Journal Letters, **413:** L105–108, 1993

[18] B. Fryxell, et. al., The Astrophysical Journal Supplement Series, **131:** 273–334, 2000 November

[19] W. Hillebrandt, New Astronomy Reviews **48**: 615–621, 2004

[20] Vadim N. Gamezo, Alexei M. Khokhlov, and Elaine S. Oran, The Astrophysical Journal, **623:** 337–346, 2005, April 10

[21] E. Hairer, G. Wanner, Solving Ordinary Differential Equations II, (Stiff and Differential-Algebraic Problems), 1991, Springer-Verlag, Berlin Heidelberg

[22] F.X. Timmes, The Astrophysical Journal Supplement Series, **124:** 241–263, 1999 September

[23] P. Colella, P.R. Woodward, J. Comp. Phys., **54:** 172–201, 1984, September

[24] F.X. Timmes, and F.D Swesty, The Astrophysical Journal Supplement Series, **126:** 501–516, 2000 February

[25] Mike Guidry, Kenneth J. Roche, Erin McMahon, and Reuben Budiardja, unpublished manuscript

[26] M.W. Guidry, O.E.B. Messer, and . Hix, and K.J. Roche, unpublished manuscript

[27] M.W. Guidry, R. Budiardja, E.Feger, W.R. Hix, O.E.B. Messer, and K.J. Roche, unpublished manuscript

[28] C. W. Gear, *Numerical Initial Value Problems in Ordinary Differential Equations*, Prentice Hall (1971)

[29] J. D. Lambert, *Numerical Methods for Ordinary Differential Equations*, Wiley (1991)

[30] W. H. Press, S. A. Teukolsky, W. T. Vettering, and B. P Flannery, *Numerical Recipes in Fortran*, Cambridge University Press (1992)

[31] E. S. Oran and J. P. Boris, *Numerical Simulation of Reactive Flow*, Cambridge University Press (2005)

[32] W. R. Hix and B. S. Meyer, to appear in special issue of Nuc. Phys. A; astro-ph/0509698

[33] T. Rauscher and F.-K. Thielemann, At. Data Nuclear Data Tables **75**, 1 (2000)

[34] R. Hix and F.-K. Thielemann, J. Comp. Appl. Math. **109**, 321 (1999)

[35] M. Ruffert and H.-Th. Janka, Astrophysics and Astronomy, **380:** 544–577, 2001

[36] A.M. Khokhlov, Journal of Computational Physics, **143(2):** 519–543, 1998

[37] F.K. Ropke, W.Hillebrandt, J.C Niemeyer, and S.E. Woosley, Astronomy and Astrophysics, **448:** 1–14, 2006

[38] P.A. Mazzali, F.K. Ropke, S. Benetti, W. Hillenbrandt, Science, **315:** 825-828, 9 February 2007

[39] F.K. Ropke, and W.Hillebrandt, arXiv:astro-ph/0409286 v1 13 Sep 2004

[40] A.C. Calder, D.M. Townsley, I.R. Seitenzahl, F. Pang, O.E.B. Messer, N.Vladimirova, E.F. Brown, J.W. Truran, and D.Q. Lamb, The Astrophysical Journal, **656:** 313–332, 2007 February 10

[41] M. Zingale, S.E. Woosley, C.A. Rendleman, M.S. Day, and J.B. Bell, The Astrophysical Journal, **632:** 1021-1034, 2005, October 20

[42] L.D. Landau, E.M. Lifshitz (1959): *Fluid Mechanics*. vol. 6 of *Course of Theoretical Physics*, Pergamon Press, Oxford

[43] M. Zingale, L.J. Dursi, The Astrophysical Journal, **656:** 333-346, 2007, February 10

[44] S.E. Woosley, S. Wunsch, M. Kuhlen. The Astrophysical Journal, **607:** 921-930, 2004, June 1

Vita

Viktor M. Chupryna was born in Ukraine on September 22, 1946. He received his Masters Degree (Equivalent) in 1964 from Kharkiv Technical University of Radio and Electronics, Kharkiv, Ukraine. In 2000 he joined the Physics and Astronomy Department of the University of Tennessee, Knoxville as a graduate student. During his study he worked both as a Graduate Teaching and as a Graduate Research Assistant. He taught undergraduate Physics labs and recitation. He did his research in the fields of astrophysics and dynamic atomic collisions. He completed his Doctoral Degree in December 2008.